Construction and Building Materials 440 (2024) 137464

Contents lists available at ScienceDirect

Construction and Building Materials

journal homepage: www.elsevier.com/locate/conbuildmat

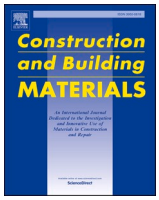

Strengthening of reinforced concrete slabs using carbon fiber reinforced polymers rods and concrete jacket with a mechanical anchorage system

Firas Hassan Saeed [a,*], Farzad Hejazi [b,*], Raizal Saifulnaz Muhammad Rashid [a]

[a] Department of Civil Engineering, University Putra Malaysia, Malaysia
[b] Faculty of Environment and Technology, The University of The West England, Bristol, United Kingdom

ARTICLE INFO

Keywords:
Reinforced concrete
Slab
Strengthening
UHPFRC jacket
CFRP rods
Mechanical anchorage system
Cyclic load

ABSTRACT

This study presented the development of a new method for strengthening of Reinforced Concrete (RC) slabs using Carbon Fiber Reinforced Polymer rods (CFRP) and an Ultra-High Performance Fiber Reinforcement Concrete (UHPFRC) external jacket with a Mechanical Anchorage System (MAS). The mechanical anchorage system includes two components: high-carbon steel plates and the Mechanical Expansion Anchorage Bolt System (MEABS), and it's employed to prevent any premature de-bonding between the existing concrete surface and the externally strengthening layers (CFRP rods and UHPFRC jacket). The efficiency of the proposed strengthening method was evaluated through conducting an experimental test on a few fortified slabs by applying cyclic loads using a dynamic actuator. For this purpose, three distinct concrete slabs were tested to assess various design parameters, including a control slab, a strengthened slab with the UHPFRC jacket only, and a strengthened slab with CFRP bars at the bottom of the slab with an external UHPFRC jacket. The results of experimental tests reveal that the proposed strengthening system significantly enhanced the load capacity of the slab and prevented premature debonding failures between the old concrete of the slab and the new UHPFRC layer until the stage of slab failure. Accordingly, the new proposed strengthening system played a crucial role in enhancing the tension zone of the slabs and delaying the occurrence of diagonal crack loads. On the other hand, embedding CFRP bars within the UHPFRC jacket in the strengthened slab led to a notable enhancement of 82 % in the ultimate load capacity of the slab. The FE and analytical models were developed to predict the behavior of the specimens. The models' outcomes were in good agreement with the experimental data. Consequently, the new proposed strengthening system emerges as a reliable technique for enhancing the performance of reinforced concrete slabs, eliminating the risk of debonding between old and new parts.

1. Introduction

Over the past few decades, the challenges associated with ageing and deterioration have become prominent issues in the construction field. Reinforced concrete structures are constructed to endure a range of environmental conditions throughout their anticipated operational lifespan. However, human errors such as changes in usage, structural design flaws, inadequate maintenance, and alterations in environmental conditions can lead to significant damage over time. These environmental factors can result in concrete deterioration, steel reinforcement corrosion, and ultimately, a loss of structural integrity [1–3]. As a result, these issues require careful consideration and innovative solutions to ensure the durability and longevity of constructed assets, and it is essential to strengthen or rehabilitate existing structures. In recent years, carbon fiber reinforced polymer (CFRP) materials have seen a notable increase in use as a strengthening technology [4–8]. CFRP materials have several benefits over other materials such as rebar steel, including high tensile strength, lightweight, fatigue strength, and corrosion resistance [9–12]. Various configurations and techniques have been developed to optimize the effectiveness of the CFRP materials, aiming to extend the service lifespan of structures [13–17]. In the domain of FRP material utilization, the Externally Bonded (EB) and near-surface mounted (NSM) techniques stand out as the principal and extensively utilized approaches. The externally bonded technique involves the attachment of FRP sheets to the tension zone or soffit of the member's surface [18,19]. In contrast, the NSM technique requires the placement of FRP reinforcement bars or strips into pre-cut grooves that are specifically positioned in the tension zone of a concrete member's

* Corresponding authors.
E-mail addresses: firashasan43@gmail.com (F.H. Saeed), farzad.hejazi@uwe.ac.uk (F. Hejazi).

https://doi.org/10.1016/j.conbuildmat.2024.137464
Received 15 March 2024; Received in revised form 8 July 2024; Accepted 11 July 2024
Available online 18 July 2024

surface [20,21]. The bonding between the CFRP bars and the adhesive, as well as the bond between the adhesive material and the concrete grooves, have a significant impact on the efficiency of the NSM process [22,23]. During cyclic loading, the CFRP does not perform effectively [24]. Ultra-high-performance fiber reinforced concrete (UHPFRC) is an innovative material that has been developed to be used for improving and strengthening reinforced concrete structures. UHPFRC material has higher compressive and tensile strengths, improved durability, enhanced ductility, and lowered permeability compared to conventional concrete [25,26]. Due to its outstanding energy absorption capacities, the UHPFRC becomes an excellent material to resist impact loads and blasts [27]. Given its exceptional mechanical and physical properties, it is promising to employ UHPFRC to improve and strengthen RC members, and numerous researchers have elaborated on the structural responses [28–30]. Yoo et al. [31] examined the effect of the longitudinal ratio of steel on UHPFRC beams, revealing that the steel fibers and rebar effectively enhance ductility and regulate crack width. Several experimental investigations combining UHPFRC and RC members have been conducted to evaluate the effectiveness of UHPFRC strengthening. Noshiravani et al. [32] assessed how reinforced concrete beams with a UHPFRC layer performed during bending. The outcomes showed that the UHPFRC layer improves structural performance, stiffness, peak loads, and cracking behavior. According to the findings of [33], strengthening of reinforced concrete beam specimens with the UHPFRC at various locations resulted in a notable enhancement in both yielding and ultimate moment capacity for all the strengthened specimens. A reinforced concrete slab strengthened by UHPC with rebar added in the layer of UHPC was tested under three-point loading, and the results revealed diagonal shear cracks in the concrete slab followed by debonding at the UHPC-concrete interface, as reported by [34]. The study conducted by [29] has demonstrated that the occurrence of slip at the interface was seen during the loading process. The possibility of premature de-bonding between the existing concrete structure and the externally added strengthening material, such as carbon fiber-reinforced polymers (CFRP), is one of the most crucial challenges for the external strengthening of concrete members. However, the construction complexity is considerably higher and CFRP also has the disadvantage of brittle fracture, potentially leading to a shear failure mode in the slab section. Therefore, it is crucial to implement an efficient and durable strengthening solution for slabs to ensure reliable bonding between the old and new materials. Accordingly, the present study focused on the development of a new strengthening technique by utilizing CFRP rods and UHPFRC jacketing at the bottom side of the slab (tensile zone) with a mechanical anchorage system. High-carbon steel plates and a mechanical expansion anchorage bolt system were used as a mechanical system to enhance the bonding of old material (RC slab) with new material (UHPFRC jacket) during the functioning and overstressing of the slab. The efficiency of the proposed retrofitting method has been assessed through experimental testing of retrofitted slabs by imposing cyclic loads. Accordingly, behavior of strengthened slabs has been investigated in terms of ultimate strength, failure modes, deflection, and cracking in comparison to the benchmark slab, and the output has been discussed.

2. Development of new strengthening method for RC slabs

2.1. Ultra-high performance fiber reinforced concrete (UHPFRC) jacketing

The UHPFRC is a significant development in composite materials and is suitable for strengthening and rehabilitating reinforced concrete (RC) structures. The UHPFRC material is a cementitious composite containing steel fibers for reinforcement, which replace traditional reinforcement steel. UHPFRC demonstrates significantly higher compressive, tensile, and flexural strengths compared to conventional concrete [25,26], enabling efficient strengthening without substantial bulk or weight. Therefore, this inherent strength improves durability, as UHPFRC is highly resistant to environmental effects such as corrosion, abrasion, and freeze-thaw cycles. Furthermore, UHPFRC has exceptional bonding properties, which ensure an excellent connection with the existing structure, reducing the possibility of delamination or debonding. Additionally, UHPFRC has the ability to be used in thin layers while maintaining its rigidity, especially in situations where space is limited. The UHPFRC jackets are more suited for reinforcing RC members with a high axial compression ratio compared to the ECC jackets, because the UHPFRC has an extremely high compressive strength. However, ECC's durability may be degraded in severe conditions, leading to concerns regarding its reliability, efficiency, and stability. UHPFRCC often exhibits superior freeze-thaw and fire resistance compared to ECC [35]. The optimal thickness of the UHPFRC layer depends on a variety of criteria, such as structural requirements, design objectives, and existing structural conditions. The UHPFRC jacketing in the currently proposed strengthening method effectively transfers stress from the concrete slab to the CFRP rods. The thickness of the UHPFRC strengthening layer increases, providing more resistance to punching shear [36]. The inclusion of extra material enhances the depth over which the load can be distributed, hence increasing the punching shear capacity of the slab. On the other hand, increasing the thickness of the UHPFRC layer helps reduce shear stress in the slab's crucial regions. A decrease in shear stress can delay or avoid punching shear failure, enhancing the slab's overall structural performance and durability. In addition, with the 50 mm thickness of the UHPFRC layer, the failure mode transitioned from a brittle diagonal shear to a ductile flexure compared to a small thickness of UHPFRC [34]. Therefore, this study used a 50-mm thickness of UHPFRC jacketing to provide sufficient strengthening to effectively enhance the structural capacity and performance of slabs (Fig. 1(a,e)). However, the cost and extra weight of the slab due to the UHPFRC jacketing are deemed undesirable issues. Future studies should evaluate how reducing the thickness of the UHPFRC jacketing affects the overall slab performance using the new proposed strengthening system. In this study, no bonding materials such as epoxy were used between the RC slab and the UHPFRC jacketing to assess the performance and effectiveness of the mechanical anchorage bonding system.

2.2. Embedded carbon fiber reinforced polymer (CFRP)

The Carbon Fiber Reinforced Polymer (CFRP) bars were used in this study as embedded in UHPFRC jacketing for strengthening the slab, as shown in Fig. 1(d). The utilization of CFRP rods in this investigation was motivated by their high modulus of elasticity, which leads to less deformation under load as compared to steel reinforcing bars. This stiffness can allow for control of deflections and enhance the overall performance of the strengthened slab. Additionally, their higher strength, lightweight, and corrosion resistance make the CFRP rods a flexible and effective solution for improving the performance and durability of reinforced concrete structures. To ensure enough bonding length and fixity in the position, the CFRP bars were extended approximately 30 mm from the mould's edge in both directions. The distribution of the CFRP rods has been carefully designed so that it does not interfere with the arrangement of the anchored bolts. In the currently proposed strengthening method, the external jackets of the UHPFRC effectively transfer stress from the existing RC slab to the embedded CFRP mesh because of its high strength. On the other hand, the mechanical properties of UHPFRC lead to a strong bond with the existing concrete slab, reducing the risk of early debonding. The exceptional workability, compaction, and self-consolidation of UHPC enhance its capability of filling the pores on the substrate surface [9]. This ability improves the capillary suction in the substrate and directly affects the sufficient contact area between UHPC and substrate. Furthermore, the UHPFRC jacket serves a crucial function in protecting the CFRP rods against environmental factors such as corrosion and fire, owing to its high resistance. In addition, Fig. 1(d) depicts the distribution of CFRP

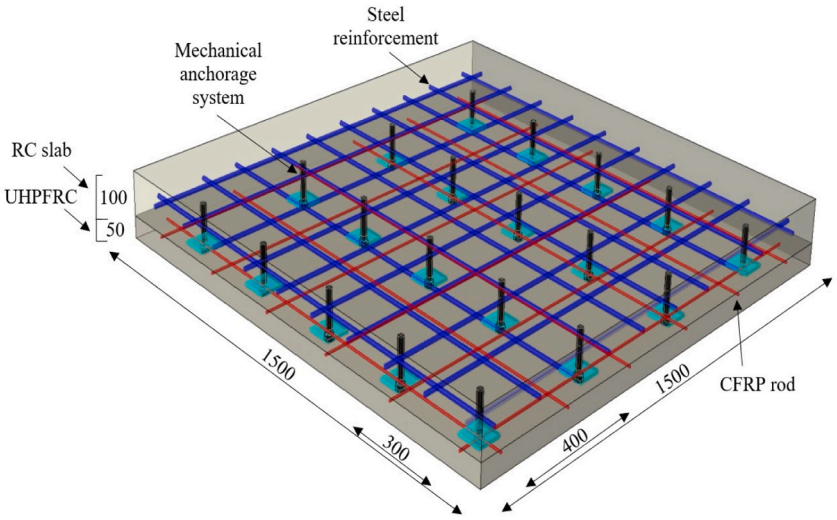

a. Details of the strengthened slab

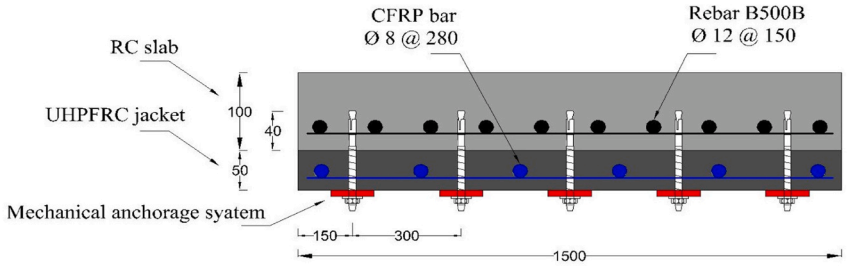

b. Cross section of the strengthened slab

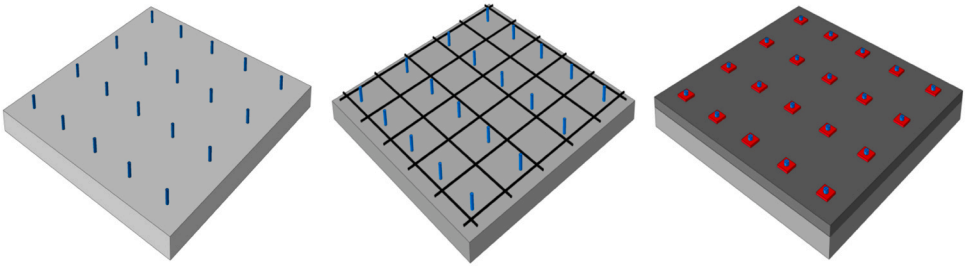

c. Installed the MEABS in the RC slab

d. Distribution of the CFRP rods

e. Bottom view after casting UHPFRC jacket and fixed the steel plates

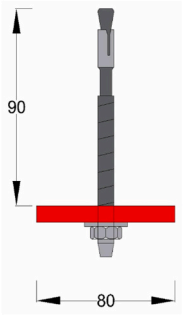

f. Carbon steel plate (80×80×10) mm

g. Mechanical Expansion Anchorage Bolts System (MEABS)

h. Mechanical Anchorage System

Fig. 1. Components of the newly proposed strengthening method.

mesh in the slab.

2.3. Mechanical anchorage system

As mentioned before, the employed mechanical anchorage system in this study consisted of Mechanical Expansion Anchorage Bolts System (MEABS) and carbon steel plate (Fig. 1(h)) which have been demonstrated as follow:

2.3.1. Mechanical expansion anchorage bolts system (MEABS)

The effectiveness of the proposed strengthening method relies on choosing the appropriate Mechanical Expansion Anchorage Bolts System (MEABS) to securely bind the existing concrete surface of the slab with the UHPFRC jacket surfaces (Fig. 1(c)). Therefore, the mechanical expansion anchorage bolt system was acquired with the specified size to ensure adequate anchorage and the appropriate amount of strength. For this purpose, the HAS-BW M12 mechanical expansion anchorage bolt system with a height of 160 mm and a diameter of 12 mm was chosen in this study (Fig. 1(g)). On the other hand, according to the ACI Guide for the design of anchorage for concrete [35], the embedding depth of the mechanical expansion anchorage bolt system in the concrete is considered one of the most critical requirements in the proposed design. Therefore, according to the mentioned code, the embedded depth of 40 mm is considered for the slabs in this study (Fig. 1(b)) since the normal strength concrete (C30/37) has been used for the cast of slabs. According to the manufacturer's report [38], the distance between the center of the mechanical expansion anchorage bolt system and the exterior edge of the slab specimen is considered to be 150 mm (Fig. 1 (b)).

2.3.2. Carbon steel plate

The second component of the suggested mechanical anchorage system is the carbon steel plates, which are designed according to ASTM A29 [39]. Its design relies on predicted forces and stresses across different loading conditions. This study used carbon steel plates to provide an appropriate bond between the UHPFRC jacket and the existing RC slab with adequate strength. Using the carbon steel plates as part of the mechanical system in this study assists in distributing applied loads more evenly throughout the surface area of the concrete substrate. This helps to avoid localized stress concentrations, decreasing the chance of premature collapse or deformation of the concrete structure. In addition, the contact area between the mechanical system and the surface of the UHPFRC jacket has significantly increased. This larger anchorage area improves the effectiveness of the mechanical anchorage system, enhancing its ability to resist applied loads and the separation of the strengthening material from the substrate. On the other hand, carbon steel offers a combination of durability, strength, and corrosion resistance, making it well suited for use in structural strengthening applications. These plates were securely fastened to the UHPFRS's bottom. face without any gap (Fig. 1(e)). The carbon steel plate had a thickness of 10 mm and dimensions of 80×80 mm, as illustrated in Fig. 1(f). A circular hole was made in the plate's center, with dimensions closely matching the diameter of the mechanical expansion anchorage bolt system (MEABS). The spacing between the two steel plates was 400 mm center to center, and 300 mm in the other direction, as shown in Fig. 1 (a). A total of twenty carbon steel plates were used in each of the specimens.

3. Experimental

3.1. Description of test specimens

For the experimental test in this study, a concrete slab was jacketed with an ultra-high-performance fiber-reinforced concrete (UHPFRC) jacket and CFRP rods bonded using a mechanical anchorage system. The proposed strengthening method comprises of CFRP bars and UHPFRC jacketing with a mechanical anchoring system. This mechanical anchorage system in the proposed strengthening technique consists of the Mechanical Expansion Anchorage Bolt System (MEABS) and carbon steel plates. Therefore, three specimens have been considered for experimental tests in this study: i) the benchmark slab (without any strengthening) (SB1); ii) the strengthened slab with the UHPFRC jacket (without CFRP bars) and mechanical bonding system (SB2); iii) the strengthened slab by an external UHPFRC jacketing with embedded CFRP bars within the jacket and mechanical bonding system (SB3). Due to limitations in the experimental laboratory, the size of all three slabs shared identical dimensions of 1500×1500×100 mm. The RC slabs are designed with accordance to ACI-318–08 and EC2. Each of the slabs was 100 mm in thickness and reinforced with a single layer of high-tensile steel reinforcement mesh (longitudinal and transverse ∅ 12), positioned at 150 mm intervals in two directions at 25 mm from each bottom of the slab. Fig. 2 shows the slab's cross-sectional and longitudinal dimensions, along with the main parameters.

As for the external strengthening jackets, the UHPFRC jacket, with a thickness of 50 mm, was used, as mentioned above in Section 2.1. The layer of UHPFRC in the SB3 specimen was reinforced with one layer of CFRP bar mesh to assess the impacts of the CFRP bars on the behavior of the strengthened slab. Because their high strength, lightweight, and corrosion resistance make the CFRP rods a flexible and effective solution for improving the performance and durability of reinforced concrete structures. The 8-mm-diameter (Sika® CarboDur® BC8) Carbon Fiber Reinforced Polymer bars were used in this study for the strengthening of the slab (Fig. 3). The proposed technique effectively controlled the bond between the hardened and new fresh concrete using a mechanical anchorage system. The employed mechanical anchorage system in this study consisted of the Mechanical Expansion Anchorage Bolts System (MEABS) and carbon steel plate. A mechanical expansion anchor bolt system (MEABS) with a length of 160 mm and a 12 mm diameter was used to bond between the UHPFRC jacket and RC slab. Twenty MEABS were embedded in each of the specimens (SB2 and SB3). The spacing between the two MEABS was 400 mm center to center, and 300 mm in the other direction (Fig. 3(b)). The effective embedded depth into the RC slabs was 40 mm, according to the ACI Guide for the Design of Anchorage for Concrete [37]. As a result, the MEABS were used in order to securely fasten the steel plates onto the bottom surface of the UHPFRC jacket. The carbon steel plate used in this investigation measured 80×80×10 mm and had a hole in the center with dimensions closely matching the diameter of the MEABS. Before conducting the test, all specimens were painted white to enhance the visibility of the initial cracks. The cross-sectional and detailed details of the strengthened slabs are shown in Fig. 3. The proposed system is poised to improve the structural integrity and durability of the slab, aligning with key aspects of current engineering standards and building codes. The UHPFRC jacket, which is one of the main components of the proposed system, was designed and implemented in accordance with the ACI 239R-18 in terms of the mixture design of UHPFRC and the protocol mixing and the curing process. While the mechanical anchorage systems, are considered one of the important elements because they are responsible for the strength of the bond between the RC slab and the UHPFRC jacket. Therefore, the embedded depth and the distribution of the bolts are among the important factors that were taken into account during the design and are aligned with existing standard ACI 355.2 and the manufacturer's report [38], ensuring that mechanical bolts meet essential criteria for safety and reliability. This comprehensive approach ensures that the proposed system aligns with current engineering standards and building codes and also delivers a robust and resilient solution for enhancing the load-carrying capacity and longevity of the RC slab.

3.2. Material properties

The following sections describe the material properties used to fabricate the slabs for the experimental tests.

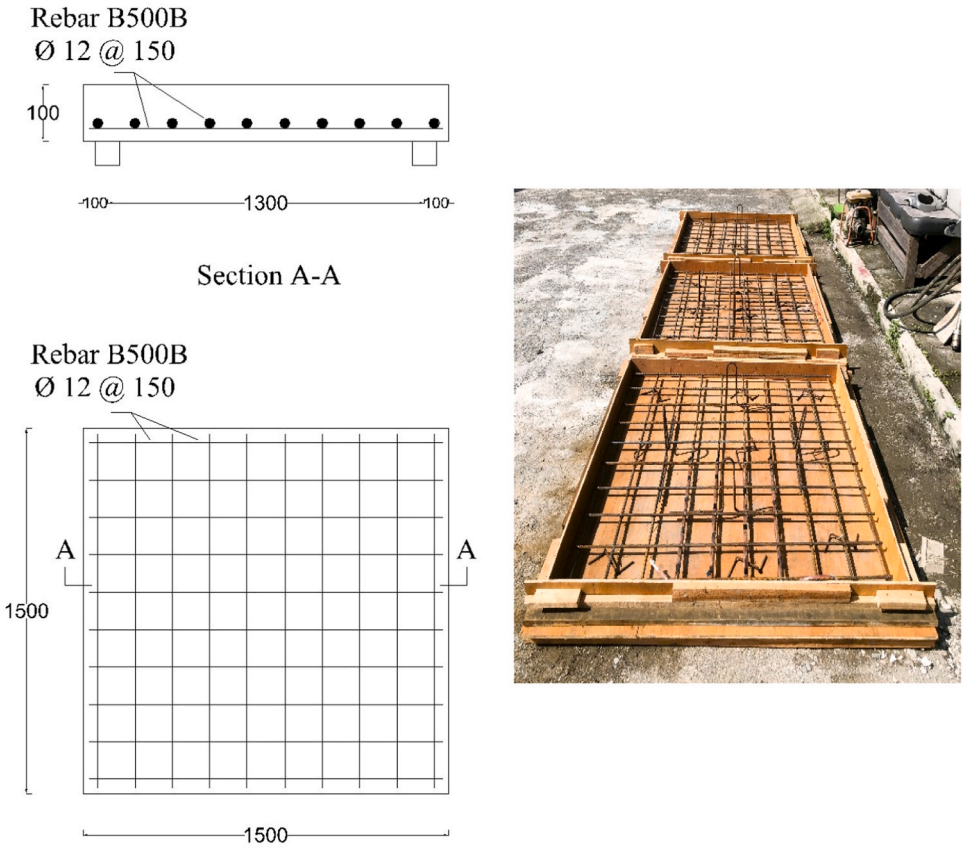

Fig. 2. Details of RC slabs.

3.2.1. Concrete

Ready-mix concrete supplied by a local manufacturer with a (C30/37) compressive strength was used to cast the three slabs. A total of nine concrete cubes, each measuring (150 ×150 ×150) mm, were manufactured in a single batch in order to assure uniform compressive strength of the concrete. Each of the three cubes was tested at 7, 14, and 28 days. The mean compressive strength of the cubes at the end of the 28-day period was recorded as 34.8 MPa. The data collected from the laboratory testing is presented in Table 1.

3.2.2. UHPFRC material

The ultra-high performance fiber reinforced concrete (UHPFRC) grade 144 MPa (average cube compressive strength) was mixed in the laboratory employing a fully automated mixer. UHPFRC is composed of a significant proportion of ordinary portland cement, micro silica, steel fibers, fine sand, water, and a high-range water-reducing admixture (DURA-ADX2813). During the mixing of the UHPFRC, the temperature was approximately 22°C. On the other hand, prior to starting the mixing, all dry and wet batch components were weighed and measured. Mixing the dry materials (cement, fine sand, and silica fume) for two minutes to homogenize the whole collected dry volume. Incorporating 90 % water and 100 % admixture into the batch over a four-minute time span. The time taken can differ as it depends on mixer efficiency and power input, and the remaining 10 % water is added to the wet ingredient (if needed) once agglomeration of premix is evident. The final stage involves incorporating steel fibers into the mixture once the initial wet mixing phase is complete, ensuring that the fibers are uniformly dispersed throughout the mixture. The mixer was discharged for 2–4 minutes following the completion of the fiber addition. Fibers should be thoroughly dispersed and an acceptable rheology realized prior to discharge. A steel fiber with a length of 20 mm was used with more than 2500 MPa tensile strength. The average compressive strength of the cubes was calculated at 7, 14, and 28 days using (150 x 150 x 150) mm cubes, as shown in Table 1. The UHPFRC mixture proportion is presented in Table 2.

3.2.3. Steel reinforcement

The concrete slab panels were reinforced with ribbed steel rebars. High-strength steel 12 mm in diameter (B500B) yielding 600 MPa and an elastic modulus of elasticity of 210 GPa was used as internal reinforcement for all slabs. Table 3 presents the mechanical characteristics of steel reinforcement bars, whereas Fig. 1 illustrates the distribution of the rebar.

3.2.4. CFRP bars

The Carbon Fiber Reinforced Polymer (CFRP) with 8 mm-diameter (CarboDur® BC8) bars were used in this study as embedded in the UHPFRC jacketing for strengthening the slab**.** These bars had a tensile strength of 2500 MPa, with young's modulus and poison's ratio of 153 GPa and 0.2, respectively. Table 4 presents the properties of CFRP bars, as obtained by the manufacturer's report [40].

3.2.5. Mechanical expansion anchorage bolts system (MEABS) and carbon steel plate

The carbon steel plates (S50C) were made of carbon steel by a local workshop. The steel consists of more than 0.4 % carbon and it characterized by having good wear resistance and average ductility. Table 3 shows the properties of the carbon steel plates. While the mechanical expansion anchor bolts with a height of 160 mm and a diameter of 12 mm were used in the study, namely the HAS-BW M12 model, and obtained from the Hilti Company. The bolt, sleeve, washer, and hexagon nut were all fabricated using carbon steel. The mechanical characteristics of mechanical expansion anchor bolt system are presented in Table 5, which has been collected from the manufacturer's report [38].

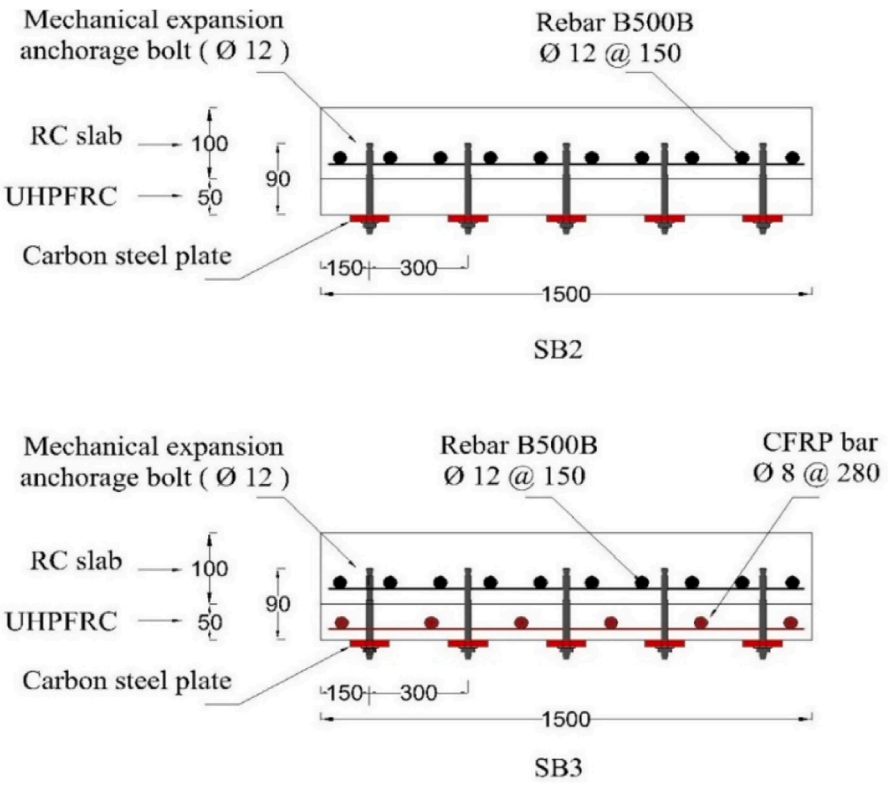

a. Cross section of strengthened slabs

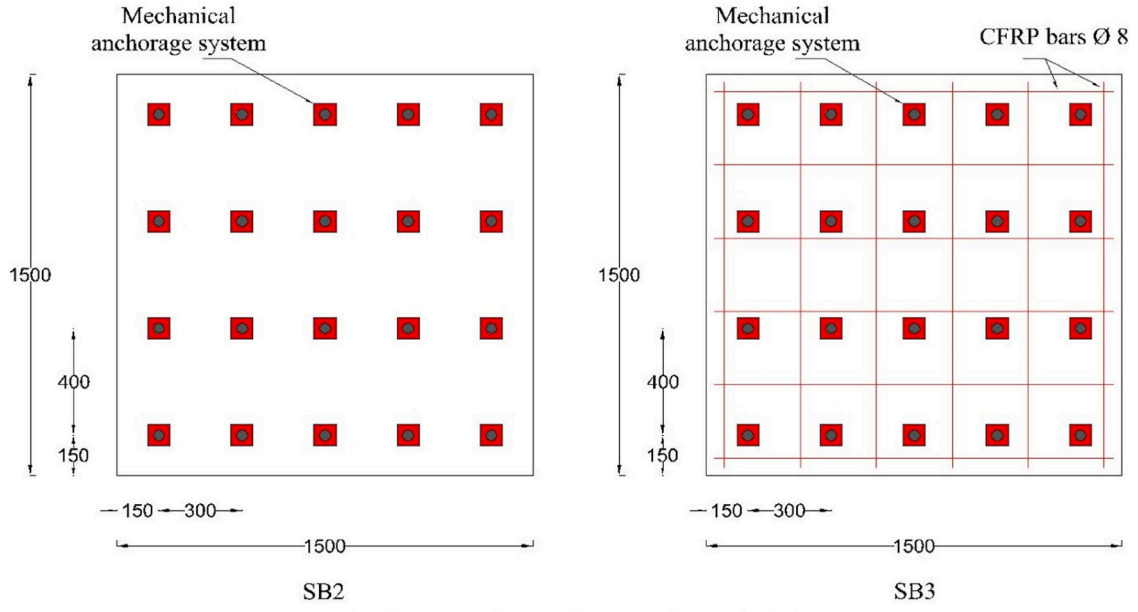

b. Bottom face of strengthened slabs

Fig. 3. Details of strengthened specimens.

3.3. Fabricating and cast the slabs

The slab specimens were constructed in the Engineering Faculty's Structural and Material Laboratory at the University Putra Malaysia. The initial step contained the detailed preparation of formwork to match the intended dimensions of the slab, which measured (1500×1500×100) mm. After that, longitudinal and transverse steel bars were arranged in the mould, and strain gauges on the center of the rebar were installed. Subsequently, the process involves pouring the concrete into these moulds and utilizing mechanical vibration techniques to achieve an ideal level of compaction, hence eliminating any possible air voids. The last stage involves curing the specimens for 28 days by spraying water and keeping the surface wet. Fig. 4 illustrates all processes of casting the reinforced concrete slabs.

Table 1
Compressive strength of Concrete and UHPFRC used in this study.

Mix		Concrete	UHPFRC
Cube specimens	Day	Ultimate compressive strength (MPa)	
1	7	27.3	110.3
2		27.6	109.6
3		26.9	111.7
4	14	31.2	138.2
5		30.3	139.4
6		31.4	137.1
7	28	34	142.3
8		34.6	144.6
9		35.9	145.7
Average (f'c) after 28 days		34.8	144.2

Table 2
Mixture design of UHPFRC.

Mix component	Amount (kg/m3)
Premix Dura	560
High-range water-reducing admixture (DURA-ADX2813)	6.832
Steel fiber (20 mm length, 0.2 mm diameter, tensile strength 2500 MPa)	42 (2 % by vol.)
Water	47.6

Table 3
Properties of steel.

Properties	Steel Reinforcement	Carbon Steel Plates (S50C)
Density (kg/m3)	7850	7860
Young's Modulus of Elasticity, E (GPa)	210	207
Poisson's Ratio, ν	0.25	0.29
Yield Strength (MPa)	600	425

Table 4
Characteristics of CFRP bars.

Characteristics	
Fiber volumetric content (%)	> 68 %
Tensile strength (MPa)	2500
Tensile modulus of elasticity (GPa)	153
Poison's ratio	0.2
Bond strength (Mpa)	18.4
Elongation at break (%)	1.6
Glass transition temperature	> 100 °C
Nominal cross-sectional area (mm2)	50

Table 5
Mechanical Expansion Anchor Bolt System (MEABS) properties.

Characteristics	
Nominal tensile strength (N/ mm2)	700
Yield strength (N/ mm2)	560
Modulus of elasticity (GPa)	206
Poison's ratio	0.28
Bond strength (Mpa)	13.7
Stressed cross-section (mm2)	84.3
Moment of resistance (mm3)	109.2
Char. bending resistance	76
Effective anchorage bolts	100

3.4. MEABS installation and carbon steel plates

The effectiveness of the proposed strengthening system relies on choosing suitable mechanical expansion anchor bolts to secure a good bonding between the existing concrete slab and the new UHPFRC jacket. In this study, HAS-BW M12 bolts were employed. The installation of the mechanical expansion anchor bolts system followed these steps: (1) identifying the designated positions of the mechanical expansion anchor bolts on the bottom face of the RC slab as per the proposed design; (2) drilling holes using a hammer with 40 mm in depth Fig. 5. (a); (3) clearing the boreholes of any debris; (4) embedding the MEABS with a hammer Fig. 5. (b); (5) sealing the upper side of the holes with silicon to prevent water ingress; (6) once the UHPFRC jacket had been cast and reached the 28-day curing period, the carbon steel plates and nuts were securely fastened to the bottom surface of the UHPFRC jacket Fig. 5. (c). One of the most important measures taken while installing the anchorage bolts is to control as much as possible the verticality of the holes that were drilled on the RC slab surface for the purpose of avoiding any gap between the top surface of UHPFRC jacket, the carbon steel plate and the nut. Refer to Fig. 5 for a visual representation of all stages of the mechanical anchorage system installation process.

3.5. UHPFRC jacket casting

After installing the mechanical expansion anchorage bolt system (MEABS) on the bottom surface of RC slabs, the UHPFRC jackets were fabricated to create the required border using wooden plates. Each of the UHPFRC jackets was 50 mm in thickness and the SB3 slab was reinforced with CFRP bars (longitudinal and transverse ∅ 8), positioned at 280 mm intervals in two directions at 30 mm from the bottom of the slab (Figs. 3(b) and 6). Due to its lightweight, the CFRP was fastened to the RC slab surface using nails after being distributed regularly and according to design, to prevent it from rising to the top while pouring UHPFRC. In the first step, the wooden plate was treated with engine oil to reduce friction and adhesion between the specimens and the wooden plate, facilitating easier and smoother removal of the specimens without causing damage or distortion. The wooden frame extended 50 mm beyond the bottom surface of the RC slab and was attached to the RC slab using several wooden supports. To evaluate the performance and effectiveness of the mechanical anchoring bonding system in this study, the RC slab's surfaces were neither roughened or treated with binders such as epoxy before casting the UHPFRC jacketing. Subsequently, the slab's surface was moistened with water to prevent water loss due to absorption by the unsaturated concrete before casting the UHPFRC jacket. In order to achieve consistency and high quality in the casting of the UHPFRC, it is essential to accurately measure the ingredients and follow the instructions for the mixing protocol of the UHPFRC, as mentioned above in Section 3.2.2. The UHPFRC was manually prepared in the laboratory. Then, the UHPFRC was slowly and carefully cast. After the UHPFRC hardened, the moulds were removed, covered by wraps, and sprayed with water periodically for 28 days. Fig. 6 demonstrates all processes for casting the UHPFRC.(Fig. 7)

3.6. Loading and test setup

This study evaluated the performance of strengthened reinforced concrete slabs with the proposed strengthening method under half-cyclic repeated loads. The cyclic load was applied with an MTS hydraulic jack mounted with a servo valve capable of bearing loads of up to 1000 KN (Fig. 8). The jack's actuator, which was vertically located within the supporting steel frame, was controlled by a Shimadzu 4830 digital smart servo controller. The cyclic load is applied by the pushing and unloading phase after the per-pushing step, permitting the jack head to return to its zero position according to the same loading rate. The loading was applied under a half-cyclic displacement-controlled test following the guidelines provided by ACI Committee 374.1–05 (ATC

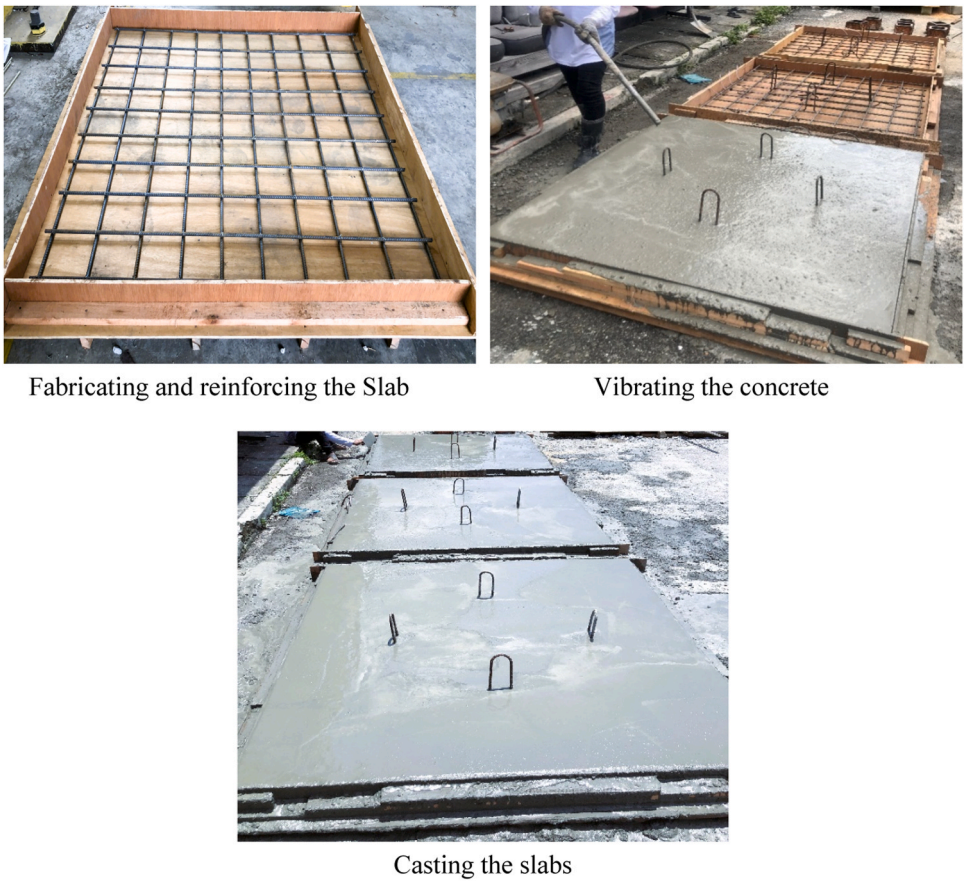

Fig. 4. Processes of casting the reinforced concrete slabs.

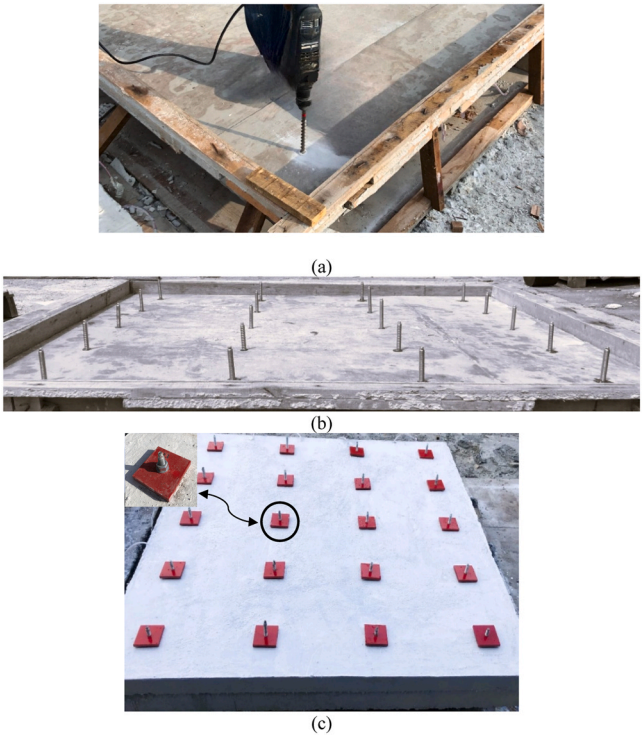

Fig. 5. Installation of the mechanical anchorage system (a) drilling holes (b) embedding MEABS (c) fastened the carbon steel plates and nuts.

1996), as shown in Fig. 7. In this method, a predetermined displacement time history was provided and entered into the controller. The controller operated the actuator according to the specified timetable, while also measuring the required load for achieving the desired movement at every (0.01 s) interval. The vertical displacement was directed downwards in the compression direction, beginning at 2 mm and increasing at a rate of 2 mm/cycle until failure. To ensure stable behavior during the test process, each loading cycle was repeated three times. This repetition loading was performed to verify the consistent behavior of the slab under a loading rate of 2 mm/m. On the other hand, two types of instrumentation were used, three electronic Linear Variable Differential Transducers (LVDTs) at the middle and each quarter to measure deflections of the slab and electrical resistance strain gauges to calculate internal rebar steel strain and concrete. (Fig. 9). A crack detection microscope meter NL 4027 X was used to measure the crack width and number in the slabs that appeared after the test. This high-definition microscope operates with an adjustable light source powered by a well-illuminated scale under all working conditions. A strain gauge with a length of 5 mm was utilised for both CFRP bar and rebar steel. Prior to affixing the gauges, the steel rebar surface underwent a polished sanding process and was subsequently cleansed with acetone solvent. Four gauges were then securely attached using cement adhesive in the middle of the CFRP rods and rebar steel in two directions. In order to avoid any potential damage to the strain gauges during the pouring process, a supplementary coating of silicone was applied to protect them. The concrete strain gauges were placed on the top (C-TS) and bottom (U-BS) surfaces at the slab's mid-point to record compression and tension strain. Two more gauges were mounted on the side faces of the slabs, one at the mid-span (C-FC) of the RC slab and the other at the UHPFRC jacket (U-FC), as shown in Fig. 9. All slabs were supported at the four edges by (200×200) mm square steel supports, and loading was applied to a

Fig. 6. Processes of casting the UHPFRC.

square steel plate (same dimensions as the supports) at the upper center of RC slabs (Fig. 8).

4. Experiment results and discussion

4.1. Ultimate strength and failure modes

Table 6 provides a comprehensive summary of the ultimate experimental loads for all slabs, along with their respective failure modes. The performance of the slabs is exhibited by the loads and the deflections at the mid-span on the bottom surface of the specimens.

Fig. 10 shows the half cyclic load versus deflection for all tested slabs. Furthermore, in order to offer a comprehensive representation of the failure behavior, the crack patterns observed in each slab are illustrated in Figs. 11,12,13. The control specimen, referred to as slab SB1, experienced flexure and crushing failure mode at an ultimate load of 164 kN, characterized by a brittle and sudden failure. This failure was displayed through longitudinal and transverse cracks in both the compression and tension zones, spanning in all four directions, as shown in Figs. 11 and 13. Notably, spalling in the concrete cover was observed on the bottom surface (tension side) of the slab, as shown in Fig. 12. On the other hand, slabs SB3 and SB2 exhibited different failure modes (Fig. 11), achieving ultimate loads of 298 kN and 264 kN, respectively, as detailed in Table 6. Consequently, it can be deduced that the ultimate

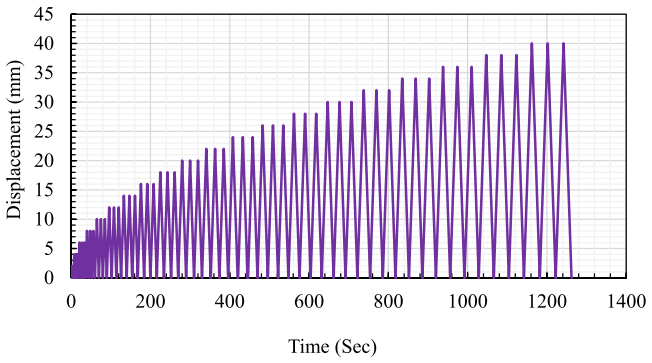

Fig. 7. Protocol of half cyclic loading.

load for the strengthened slabs increased by an average of 72 %. However, from the curves in Fig. 10, the three cyclic curves had a slight situation of stress decrease and residual displacement increase due to damage. It is possible that the material under investigation exhibits unique mechanical properties, such as high ductility or resilience, which allow it to withstand multiple loading and unloading cycles without significant damage accumulation. Another factor that may impact the observed behaviour is the speed loading rates. Due to the insufficient duration of the loading and unloading process, the specimen does not have enough time to fully revert to its original position, specifically, prior to the initial or subsequent cycle. The CFRP rod and the UHPFRC jacket with a mechanical anchorage system (MEABS and carbon steel plate) played a crucial role in enhancing the tension zone of the slabs and delaying the occurrence of diagonal crack loads, as shown in Fig. 12.

Nevertheless, slab SB2 experienced a flexure failure and concrete crushing in the compression surface, particularly in the loading zone, as shown in Fig. 13. The failure occurred when a two-main flexural crack in two opposite directions formed at the mid span and fractured through the UHPFRC jacket. One of these cracks reached the upper surface of the reinforced concrete slab layer. Whereas the SB3 slab showed a diagonal shear without any signs of concrete crushing. When four cracks developed in opposite directions, they appeared in the UHPFRC jacket at a distance of 150 mm from the middle of the slab and beside the mechanical anchorage systems. After that, failure occurred in the specimen without the cracks extending to the upper surface of the slab. Significantly, the embedding of CFRP bars into the UHPFRC jacket of the SB3 specimen led to enhanced ultimate strength compared to the SB2 slab, as

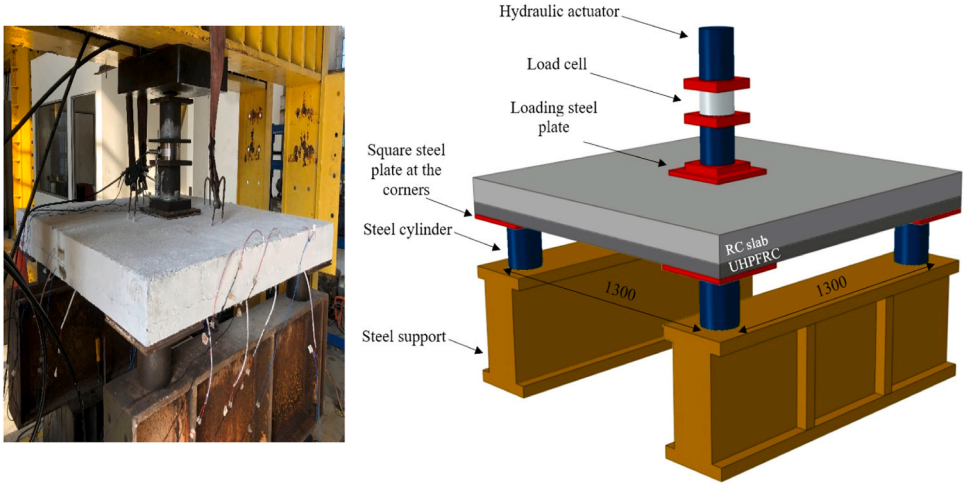

Fig. 8. Test setup for specimens.

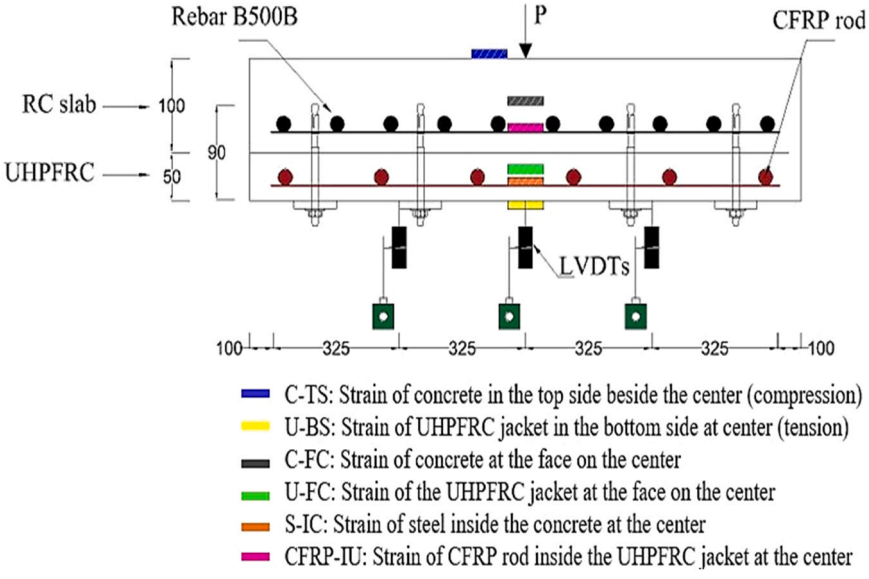

Fig. 9. Layout the location of the strain gauges and LVDTs.

Table 6
Summary of test results.

Slab ID	Pcr [kN]	δcr [mm]	Py [kN]	δy [mm]	Pu [kN]	δu [mm]	Increase in Pu [%]	μΔu [%]	Mode of failure
SB1	79	6.14	152	16	164	18	-	1.1	flexure-crushing
SB2	130	4.1	221	15	264	27	61	1.8	flexure-crushing
SB3	156	3.4	244	11	298	22.4	82	2.03	shear

Pcr: cracking Load, δcr: deflection at cracking, Py: Load at yielding of steel, δy: deflection at yielding, Pu: ultimate load, δu: deflection at ultimate load, μΔu: ductility index for deflection.

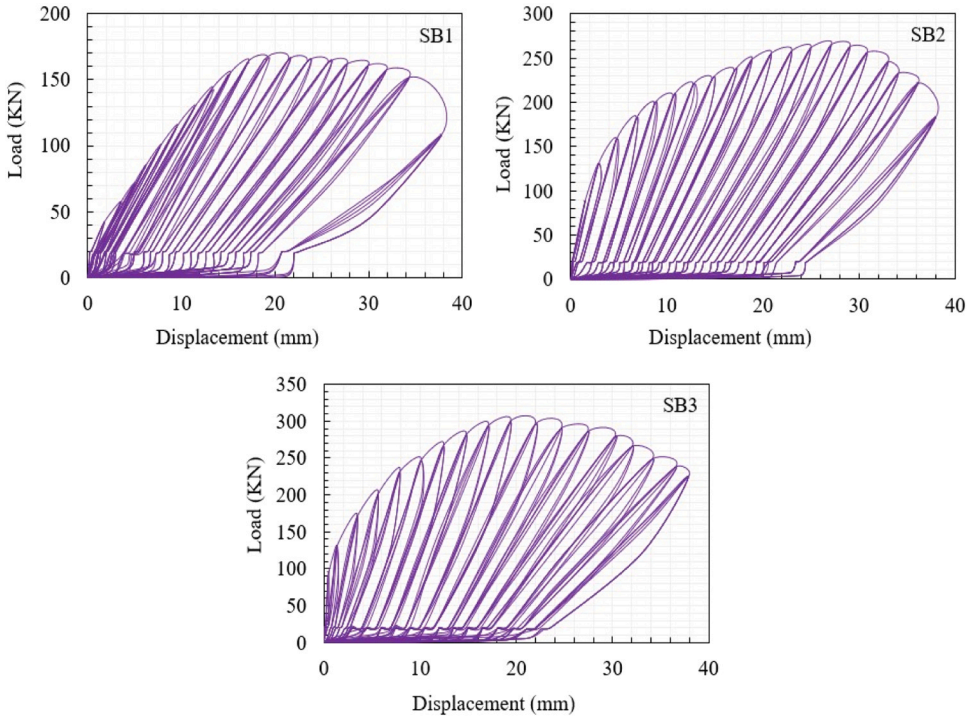

Fig. 10. Hysteretic curves of tested slab specimens.

shown in Table 6. From observations on slabs SB2 and SB3, it is clear that none of the mechanical anchorage systems experienced slippage before or during the failure of the slabs. At the same time, no debonding appeared between the RC slab and the UHPFRC jacket in both specimens (SB2 and SB3) throughout the test stages. This is mainly due to the efficiency and effectiveness of the mechanical anchorage systems that connected the two layers (RC slab and UHPFRC layer).

4.2. Load deflection behavior

Fig. 14 illustrates the load-deflection curves tested for all slab specimens. Strengthened slabs (SB2 and SB3) exhibited a notable improvement in stiffness, particularly during the later stages of the elastic, compared to the unstrengthen slab (SB1). Fig. 15. shows the load-strain of the rebar steel and CFRP rod for all specimens. The load-deflection response of slab SB1 demonstrated linearity, which is indicative of the features associated with brittle flexure failure behavior and limited ductility. The load increased linearly, with the first cracking occurring at a load level of 79 kN. Before the load reached 130 kN, lateral macro-cracks in the bottom surface of the slab developed significantly and yielded the reinforcing steel in the RC slab that occurred due to concrete crushing at the loading zone. Subsequently, it exhibited a significant reduction in stiffness and substantial deformations until failure. In contrast, slabs SB2 (without CFRP bars embedded in the UHPFRC jacket) and SB3 (incorporating CFRP rods in the UHPFRC jacket) showed different behavior from SB1 slabs. The cracking strength improved in the slabs that were strengthened with the new proposed strengthening system (SB2 and SB3), which expanded the linear range of stiffness. Whereas the load increased in SB2 and SB3 slabs with enhanced stiffness till reaching cracking stages of 130 kN and 156 kN, respectively. The superior performance of the SB3 slab, nearly doubling the initial cracking load of the control slab (SB1), attests to the efficacy of the new proposed strengthening technique. Interestingly, as shown in Table 7, the embedding of CFRP rods within the UHPFRC jacket into the SB3 slab led to an overall reduction and delayed the initiation of cracks in the slab. On the other hand, the displacements at a 100 kN load (Fig. 14) further the performance disparities: the SB2 slab exhibited a displacement of 1.7 mm, while the SB3 slab showed a significantly reduced displacement of 0.6 mm at the same load. However, in the case of the SB3 slab, the efficient distribution of stress transfer from the existing slab to the CFRP mesh led to strain curves surpassing their entire yield capacity. Also, the CFRP mesh, which acted as supplementary reinforcement within the UHPFRC layer, increased the tensile strength of the strengthened slab (SB3) and improved its flexural capacity. Additionally, the use of mechanical anchorage systems and the even distribution of mechanical anchorage systems led to an increased yield force and ultimate load. The yield stage of the SB1 slab increased from 152 kN to 221 kN and 244 kN for the SB2 and the SB3 slabs, respectively, as shown in Fig. 15. The slope of the load-deflection curve of strengthened slabs (SB2 and SB3) remained consistently greater than that of the SB1 slab from beginning to end, indicating that flexure stiffness was greater than for the unstrengthen slab (SB1). This can be attributed to the occurrence

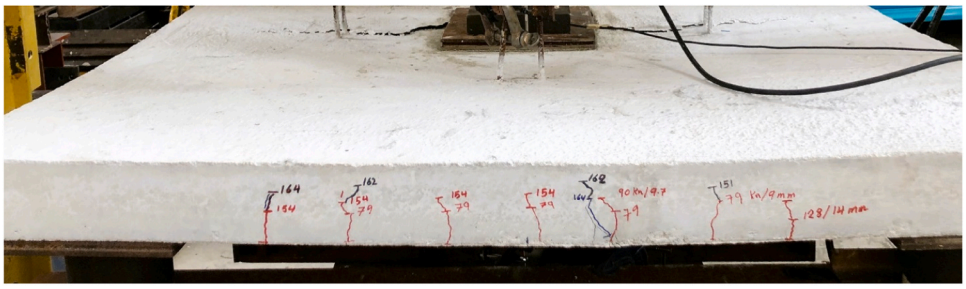

SB1

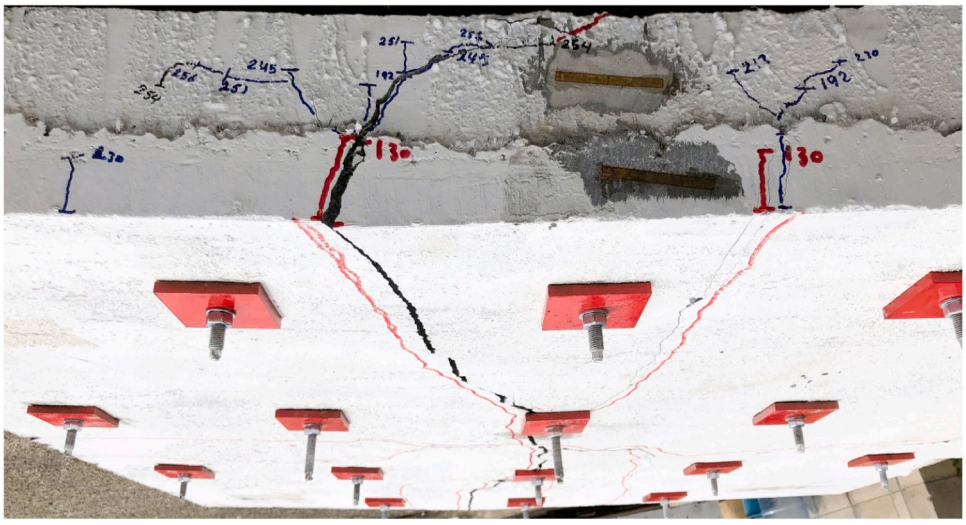

SB2

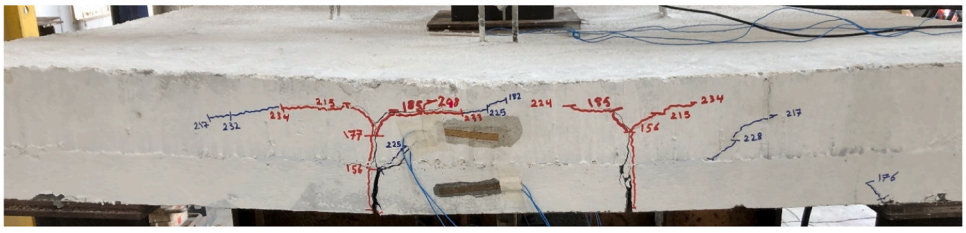

SB3

Fig. 11. Failure mode on the same side of the slab specimens.

and development of cracking in the tension zone of the SB1 slab. On the other hand, due to the separation of the steel fibers and the smoothness of the CFRP bar's surface, the CFRP bar slipped and preventing it from reaching the yield stage. The SB3 slab showed increased stiffness across all loading stages compared to the SB2 slab. Therefore, reinforcing the UHPFRC jacket with CFRP mesh resulted in a 13 % improvement in the slab's load-bearing capacity compared to the SB2 slab. These findings illustrate the effectiveness of the CFRP mesh in limiting deformations and enhancing the overall structural durability of the slab, as represented in Fig. 12. Both SB3 and SB2 slabs demonstrated a higher maximum load in comparison to the SB1 slab. Specifically, the SB2 specimen enhanced the slab capacity by 61 %, whereas the SB3 specimen improved the slab by 82 %, as shown in Table 6. On the other hand, carbon steel plates that were used in the mechanical anchorage system helped distribute the load applied by the bolt over a larger surface area of the slab and prevented localized stress concentrations that could contribute to slab deformation. Importantly, none of the mechanical anchorage systems (MEABS and carbon steel plates) experienced any slipping off the RC slab, as depicted in Fig. 12. This led to a reduction in the number of cracks and an increase in the stiffness of the slabs. Generally, the mechanical proposed strengthening technique revealed its significant contributions to increasing the ultimate load, deflection control, and the prevention of premature de-bonding. This ensures the reliability and enhanced performance of the strengthened slabs, showing the effectiveness of the proposed strengthening method.

4.3. Crack pattern

Fig. 16 illustrates the relationship between the load and the average width of the cracking observed during the experimental testing stage for all slabs. The initial cracks in the SB1 slab at 79 kN increased to 130 kN and 156 kN for the SB2 and SB3 slabs, respectively. These initial cracks were flexural and vertical lines that initiated from the bottom face of the slab to the upper, as demonstrated in Figs. 11 and 12. Hence, it can be inferred that the initial cracking load in the strengthened slabs (SB2 and SB3) exhibited an average increase of 82 %. On the other hand, the

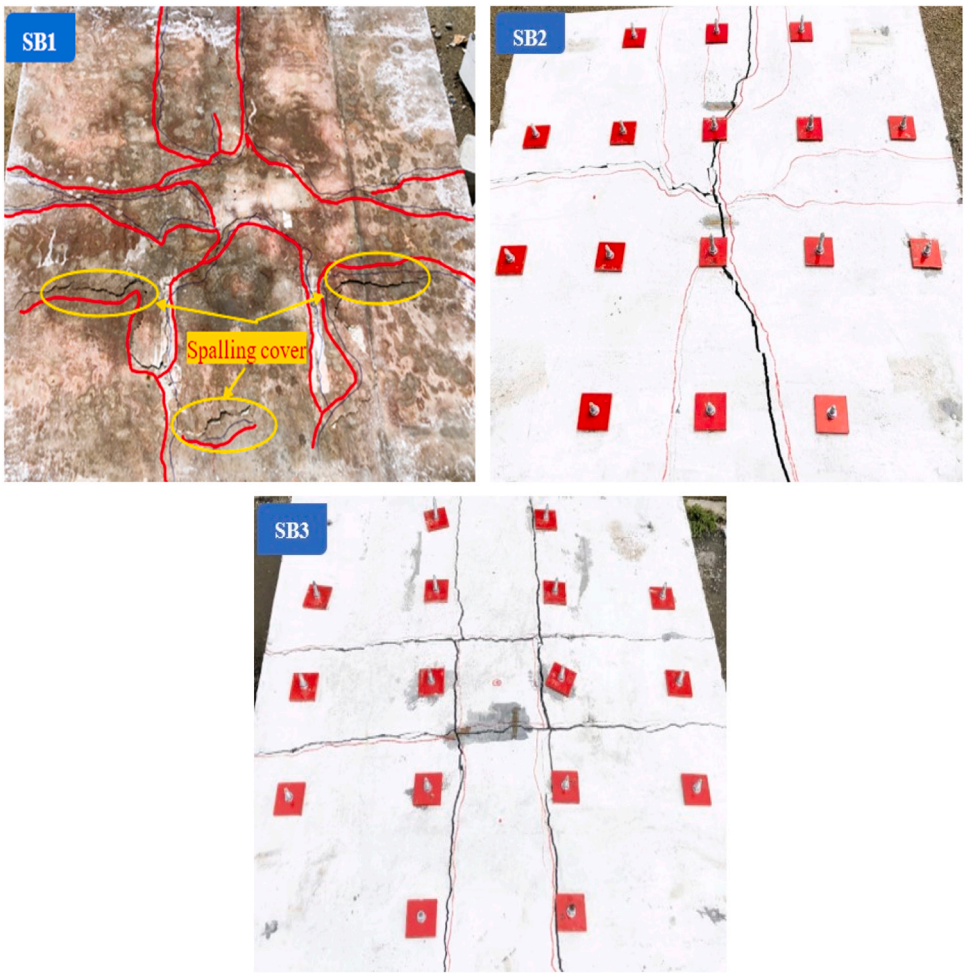

Fig. 12. Crack patterns on the bottom face (tension side) of specimens.

stiffness of the SB1 slab decreased due to concrete crushing and propagated cracks on all sides of the slab, as shown in Fig. 13. In the SB1 slab, the failure happened when at least one of the cracks in the different sides of the slab in the middle developed, spread across the bottom surface, and increased in width, as demonstrated in Fig. 12. The remaining strengthened slabs (SB2 and SB3) exhibited failure upon widening the cracks, regardless of the number of cracks present. As the load increased, cracks became obvious on all four sides of the slabs (SB2 and SB3), attributed to the energy release occurring at the center of the slabs, as shown in Fig. 13. These cracks propagated rapidly until reaching the point of collapse. The behavior of cracks can be characterized by two parameters: width and number. After reaching the maximum load, the mean crack number was calculated and accounted for all cracks that occurred on all four sides of the slab (i.e., four faces) (Fig. 11). For the SB1 slab and during the test stage leading up to the collapse of the concrete slab, the maximum width of the crack was observed to be 6.8 mm, indicating a corresponding load of 164 kN. While the maximum width of the crack for SB2 and SB3 slabs was measured at 5.12 mm and 3.9 mm at loads of 264 kN and 298 kN, respectively. The proposed strengthening method remarkably decreased the width and number of cracks in the bottom surface (tension side) of the slabs, as demonstrated in Fig. 12. Table 7 presents the crack number at the ultimate load for each specimen in the all regions.

4.4. *Ductility, energy absorption and fire resistance of the slab*

Ductility is the ability of the concrete slab to undergo plastic deformation and exceed its point of yielding without experiencing a fracture. Table 6 shows the yield (Δy) and ultimate (Δu) deflection values taken from the load versus deflection curve. In this study, the ductility index was used to assess the ductility of the strengthened slabs that followed the newly proposed strengthening system. This was achieved by comparing the SB1 slab with the SB2 and SB3 slabs. Eq. (1) was utilized to compute the deflection ductility indexes (μΔu) based on yield and ultimate deflection values, [41].

$$\mu\Delta u = \Delta u/\Delta y \tag{1}$$

Table 6 shows that SB2 and SB3 specimens have higher ductility index ratios than SB1 specimens. Specifically, the ductility index ratios for the SB2 and SB3 slabs were 1.8 and 2.03, respectively, while the SB1 slab had a ductility ratio of 1.1. Moreover, for the SB3 specimen, the embedded additional CFRP mesh at the bottom of the slab (UHPFRC jacket) led to an increase in the ultimate load and an enhancement in the slab ductility. This suggests that the newly proposed strengthening technique has notably elevated the ductility performance of the slab when compared to the control specimen (SB1). On the other hand, the energy absorption capacity of a structural element is its capability to distribute or absorb energy without failing or deforming excessively under loading conditions. The energy absorption capacities of the three slabs, SB1, SB2, and SB3, were determined by determining the area under the curve load deflection, as displayed in Fig. 14. Table 8 illustrates that SB3 exhibited the highest absorption capacity at 8428 kN. mm, along with the highest flexural value. Conversely, SB2 displayed a decrease in absorption of 435 kN.mm in comparison to SB3. The significant improvement in energy absorption capability from SB3 to SB2 indicates that the incorporation of CFRP rods in the UHPFRC jacket

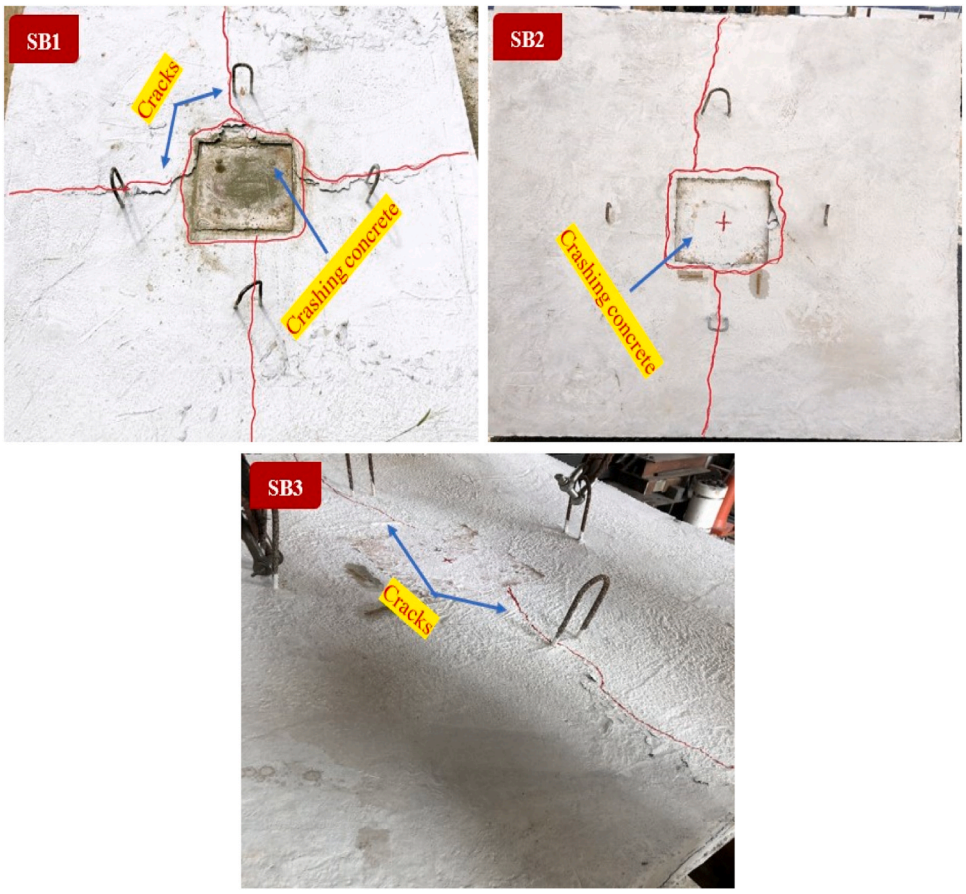

Fig. 13. Crack patterns on the top face (compressive side) of specimens.

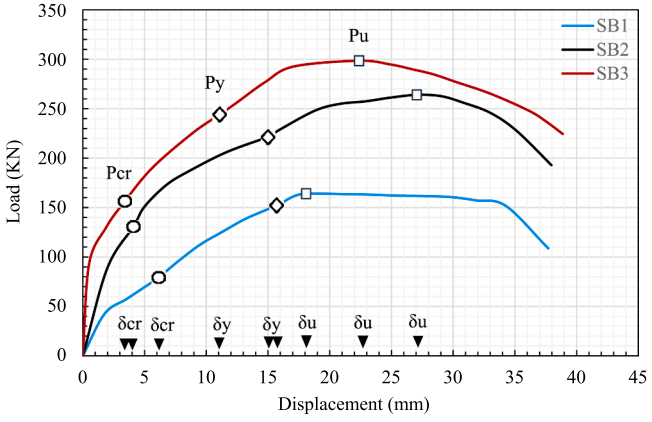

Fig. 14. Skeleton load versus mid-span deflection for all slabs.

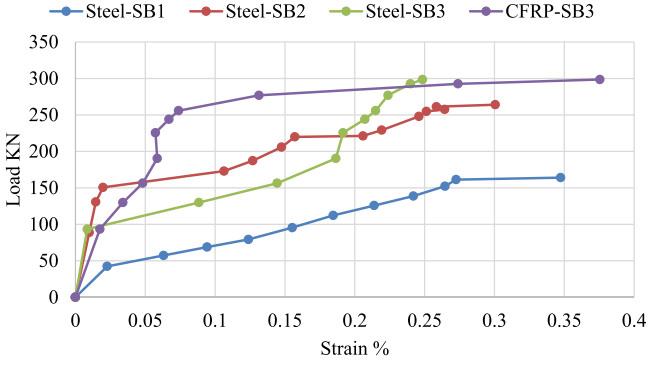

Fig. 15. Load-strain of the rebar steel and CFRP rod.

improved energy dissipation performance. Overall, the energy absorption capacity of the strengthened slabs (SB2 and SB3) increased by an average of 85 % and 95 %, respectively, compared to SB1. According to the energy absorption outcomes, the proposed strengthening method improved the energy absorption capacity of the slabs. On the other hand, the proposed method for strengthening an RC slab with a UHPFRC jacket and mechanical anchorage bolts provides many fire-resistant benefits, which contribute to increased safety and structural integrity. UHPFRC, known for its superior mechanical capabilities, has inherent fire resistance due to its high-density composition and low porosity. During fire exposure, the UHPFRC jacket maintains its structural integrity and retains its load-bearing capacity for a longer duration compared to

Table 7
Number of cracks and ultimate load.

Specimen	No. of cracks at sides region	No. of cracks at upper face	No. of cracks at bottom face	ultimate load
SB1	23	2	17	164
SB2	18	1	8	264
SB3	12	1	4	298

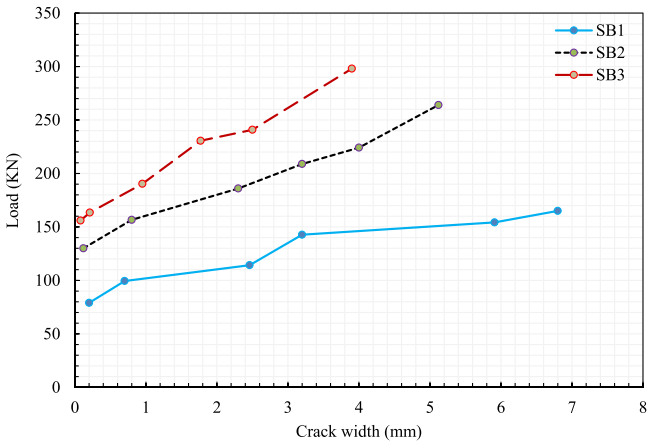

Fig. 16. The load versus crack width.

traditional concrete. Also, the mechanical anchorage systems used to connect the UHPFRC jacket provide a robust connection that helps mitigate the risk of delamination or spalling under fire conditions. Overall, the combination of UHPFRC's inherent fire resistance and the strengthening system's protective properties enhances the RC slab's fire performance.

4.5. Strain behavior

This section of the study illustrates the strain behavior of steel, CFRP rod, and concrete, as shown in Fig. 9. The strain values were determined by calculating the average values of strain gauge readings collected during the experiment. The maximum strain was measured during the test for all slabs indicated in Table 8. Fig. 17 shows the maximum strain versus ultimate load in the center of steel reinforcement and CFRP rods in all specimens. At the ultimate load level, the maximum strain of the steel reinforcement in the reinforced concrete layer of the strengthened slabs SB2 and SB3 was significantly less than that of the unstrengthen slab SB1. The strain decrease in SB2 suggests that the slab's load-carrying ability and deformation resistance have improved as a result of the external UHPFRC jacket bonding. The presence of the strengthening UHPFRC jacket allowed the tensile strength of UHPFRC to remain effective due to the bridging action of steel fiber into the UHPFRC jacket after cracking, unlike an unstrengthen slab where all tensile force was transmitted to the steel reinforcement after the RC layer cracking. Furthermore, the mechanical anchorage system used in conjunction with the UHPFRC jacket helped to improve bond strength and stress transfer between the RC slab and the UHPFRC jacket, resulting in the observed decrease in steel strain. In SB3 slab, the maximum strain of 0.002485 mm recorded in the steel reinforcement indicates a further reduction compared to both SB1 and SB2 (Table 8). This reduction is attributed to the presence of CFRP rods in the UHPFRC jacket, which enabled the steel reinforcement to better resist tensile stress. Embedding a CFRP mesh into the UHPFRC jacket improved the tensile strength and stiffness of the slab, resulting in improved crack control and load distribution. This, in turn, leads to a more effective use of the steel reinforcement and a decrease in strain. The strain response in the strengthened slabs (SB2 and SB3) illustrates the efficacy of the newly proposed strengthening system in improving the performance of reinforced concrete slabs, notably in terms of flexural capacity and deformation control by considering the behavior of tensile steel. Fig. 9 also depicts the location of the concrete strain gauge on the slabs. SB1 slab had a maximum load of 164 kN; however, the strain of concrete in the two regions (tension and compression) surface was significantly higher than that of strengthened slabs SB2 or SB3, which had approximately twice the ultimate load, as shown in Fig. 17. The strain on the compression side of the SB1 slab was 0.001347 mm/mm, corresponding to a 164 KN maximum load. This value was reduced by 8 % and 15 % in SB2 and SB3 at ultimate loadings of 258 KN and 298 KN, respectively. Besides that, the strain on the tension side of the SB2 and SB3 slabs decreased by 15 % and 24 %, respectively. It can be concluded from this that the use of the proposed strengthening system improved the compressive and tensile strength of the slabs.

Where: C-TS represents the strain of concrete in the top side (compression); U-BS represents the strain of the UHPFRC jacket in the bottom side (tension); C-FC represents the strain of concrete at the face on the center; U-FC represents the strain of the UHPFRC jacket at the face on the center; S-IC represents the strain of steel inside the concrete in the center; CFRP-IU represents the strain of CFRP rod inside the UHPFRC jacket at the center.

5. Numerical investigation

A finite element (FE) model was developed to predict the structural response of strengthened RC slabs using CFRP rods and UHPFRC external jackets with a mechanical anchorage system. This investigation used the ABAQUS software package [42] to perform the nonlinear analysis. The numerical study includes two main parts. The initial part involves modelling the slabs with identical parameters as those implemented in the experimental work, while in the second part, a parametric study is considered to assess the effectiveness of the newly proposed system. Fig. 18 illustrates the FE model's scheme for non-composite and composite slabs. The subsequent sections present the modeling procedures employed to simulate the strengthened RC slabs.

5.1. Material constitutive laws for steel and CFRP rod

Fig. 19 illustrates the stress-strain curves used to model the

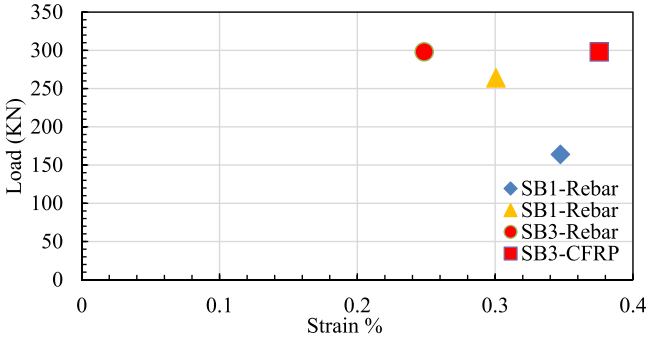

Fig. 17. Maximum strain versus ultimate load of steel reinforcement and CFRP rods.

Table 8
Maximum strain during the test for all slabs.

Slab ID		Ultimate strain at peak load					Energy absorption
	C-TS%	U-BS%	C-FC%	U-FC%	S-IC%	CFRP-IU%	KN.mm
SB1	0.1347	0.0821	0.1281	-	0.3474	-	4316
SB2	0.1243	0.0693	0.1543	0.2140	0.3006	-	7993
SB3	0.1145	0.0626	0.1750	0.3621	0.2485	0.3755	8428

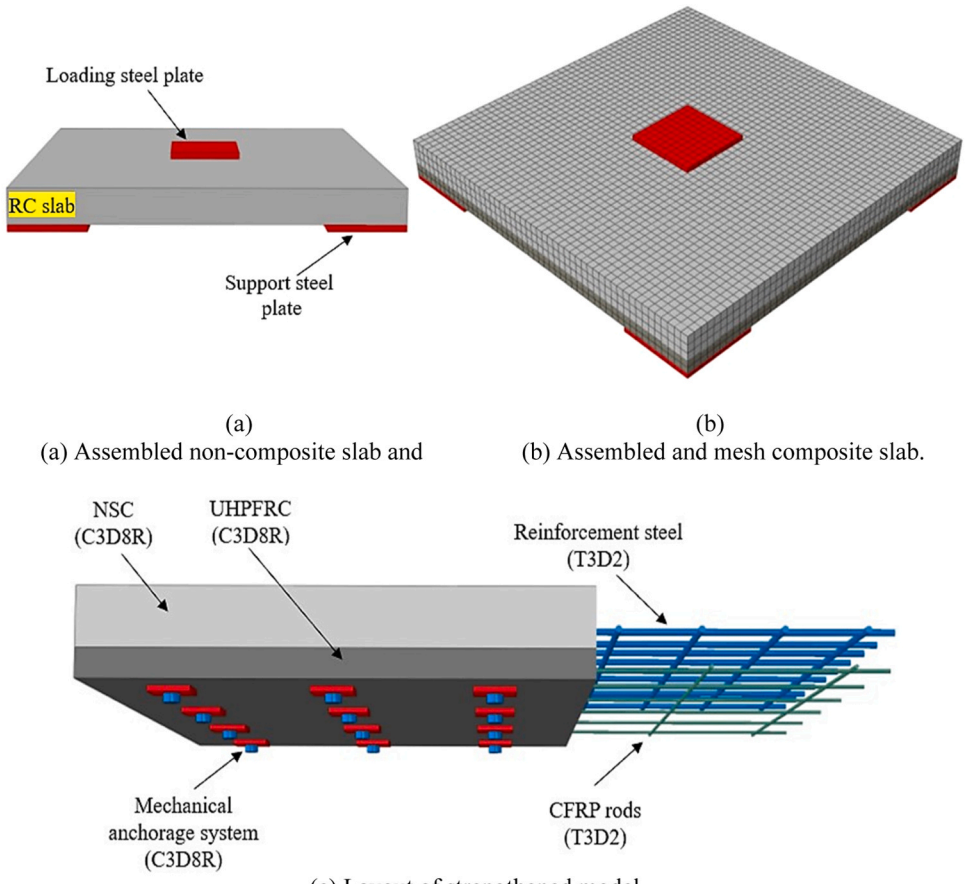

Fig. 18. Assembly and layout the FE models.

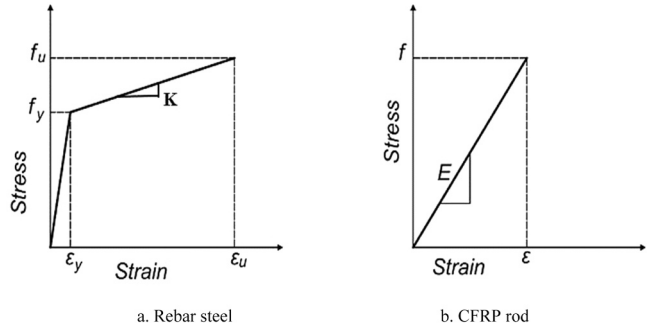

Fig. 19. Stress-strain curve used to model reinforcing steel and CFRP rods [43].

reinforcing steel and CFRP rods [43]. In the present investigation, the basic linear elastic-plastic model with strain hardening was employed for the reinforcing steel bars, as shown in Fig. 19 (a). On the other hand, the CFRP rod is modeled using an isotropic linear elastic model until failure [44], as presented in Fig. 19 (b). For the mechanical anchorage system, an elastic completely plastic model was defined for the steel plate, while the expansion anchor bolts modeled a bilinear behavior with the strain hardening, utilizing a modulus of hardening of 0.01Es [45]. Table 9 presents the mechanical properties of the reinforcing steel, CFRP rods, and mechanical system.

5.2. Constitutive model of concrete (NSC and UHPFRC)

This study employed the Concrete Damaged Plasticity (CDP) model to simulate the nonlinear behavior of both Normal Strength Concrete

Table 9
Material properties used in the FE model.

Element	Description	Value of model
NSC	Density (kg/m3	2200
	Poisson's ratio	0.19
	Compressive strength (MPa)	34
	Tensile strength (MPa)	3
UHPFRC	Density (kg/m3	2200
	Poisson's ratio	0.19
	Compressive strength (MPa)	144
	Tensile strength (MPa)	10.5
Rebar		
	Density (kg/m3)	7850
	Poisson's ratio	0.25
	Young's modulus (GPa)	210
	Yield strength (MPa)	600
CFRP rods		
	Density (g/cm3)	1.6
	Poisson's ratio	0.2
	Young's modulus (GPa)	153
Mechanical Expansion Anchorage Bolt		
	Density (kg/m3)	7860
	Poisson's ratio	0.28
	Young's modulus (GPa)	206
	Yield strength (MPa)	560
High carbon steel plate		
	Density (kg/m3)	7860
	Poisson's ratio	0.29
	Young's modulus (GPa)	207
	Yield strength (MPa)	425

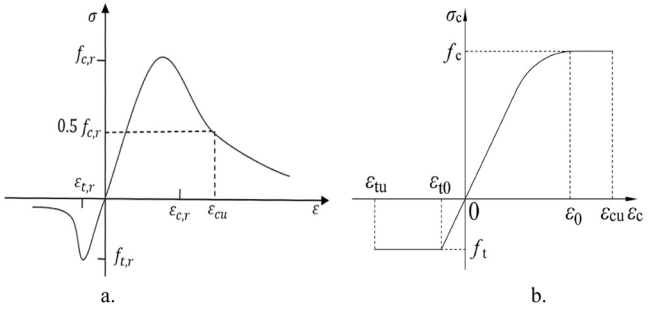

Fig. 20. Uniaxial stress-strain curve in compression and tension of (a) NSC [46] and (b) UHPFRC [47].

(NSC) and UHPFRC jackets under compression and tension conditions. Fig. 20 (a) illustrates the stress-strain curves of NSC in compression and tension [46]. The constitutive stress-strain relationships of the normal-strength concrete with a class C30/37 under uniaxial compression and tension were obtained from the code of design of concrete structures (GB50010–2010) [46]. Eqs. (2–5) provide the derivation of the constitutive law processes for NSC's tensile and compressive stress-strain relationships. In contrast, the constitutive stress-strain relationship curves of UHPFRC in both uniaxial compression and tension were obtained by L. Jia et al. [47], as shown in Fig. 20 (b). Eqs. (6–7) provide the constitutive methods for calculating the UHPFRC tensile and compressive stress-strain relationships. Based on the manual user of ABAQUS software [42], the relations between stress and strain for both UHPFRC and NSC must be transformed into stress-inelastic strain relationships. Eqs. (8) and (9) were used to calculate the inelastic strain. The concrete damage parameter in both tensile (D_t) and compressive (D_c) for NSC and UHPFRC was calculated using Eqs. 10 and 11, as given in [48]. In addition, the constitutive CDP model incorporates additional parameters to describe concrete behavior more comprehensively. Therefore, the following parameters were used in the CDP model for both NSC and UHPFRC: the viscosity parameter of 0.0001, the dilation angle of 36°, the flow potential eccentricity of 0.1, the stress ratio of invariant on tensile to the compressive meridian of 0.667, and the yield stress ratio with equal biaxial compression to the initial yield stress under uniaxial compression of 1.16 [49–51]. Table 9 presents the mechanical properties of the NSC and UHPFRC.

$$\sigma = (1 - d_t) E_c \varepsilon \tag{2}$$

$$d_t = \begin{cases} 1 - \rho_t \left[1.2 - 0.2x^5\right] & x \le 1 \\ 1 - \dfrac{\rho_t}{\alpha_t (x-1)^{1.7} + x} & x > 1 \end{cases} \tag{3}$$

$$X = \frac{\varepsilon}{\varepsilon_{t,r}}; \rho_t = \frac{f_{t,r}}{E_c \varepsilon_{t,r}}$$

$$\sigma = (1 - d_c) E_c \varepsilon \tag{4}$$

$$d_c = \begin{cases} 1 - \dfrac{\rho_c n}{n - 1 + x^n} & x \le 1 \\ 1 - \dfrac{\rho_c}{\alpha_c (x-1)^2 + x} & x > 1 \end{cases} \tag{5}$$

$$\rho_c = \frac{f_{c,r}}{E_c \varepsilon_{c,r}};\ n = \frac{E_c \varepsilon_{c,r}}{E_c \varepsilon_{c,r} - f_{c,r}};\ X = \frac{\varepsilon}{\varepsilon_{c,r}}$$

Where; $f_{t,r}$ denotes tensile strength of NSC; $f_{c,r}$ denotes the NSC compressive strength; $\varepsilon_{t,r}$ denotes the NSC tensile strain corresponding to $f_{t,r}$; $\varepsilon_{c,r}$ denotes the NSC compressive strain corresponding to the $f_{c,r}$; Ec denotes the NSC elastic modulus; d_t denotes the tensile factor of concrete; d_c denotes the compressive factor of NSC.

$$\sigma_{c,c} = \begin{cases} f_c \dfrac{n\xi - \xi^2}{1 + (n-2)\xi} & 0 < \varepsilon \le \varepsilon_0 \\ f_c & \varepsilon_0 \le \varepsilon_{c,c} \le \varepsilon_{cu} \end{cases} \tag{6}$$

$$n = \frac{Ec}{Es}; \xi = \frac{\varepsilon_{cu}}{\varepsilon_0}$$

$$\sigma_{c,t} = \begin{cases} f_t \dfrac{\varepsilon_t}{\varepsilon_{t0}} & 0 < \varepsilon_{c,t} \le \varepsilon_{t0} \\ f_t & \varepsilon_{t0} < \varepsilon_{c,t} \le \varepsilon_{tu} \end{cases} \tag{7}$$

$$\varepsilon_{t0} = \frac{f_t}{Ec}; \varepsilon_{tu} = \frac{30\ f_t}{Ec}$$

Where: f_c represents the compressive strength of UHPFRC; f_t represents tensile strength of UHPFRC; Ec represents the elastic modulus of UHPFRC; Es is the equivalent secant modulus at peak state; ε_{cu} represents the ultimate compression strain; ε_0 represents the peak compression strain at f_c; ε_{t0} represents peak tension strain at f_t; ε_{tu} represents the ultimate tension strain of UHPFRC.

$$\varepsilon_c^{in} = \varepsilon_c - \sigma_c / E_0 \tag{8}$$

$$\varepsilon_t^{in} = \varepsilon_t - \sigma_t / E_0 \tag{9}$$

$$D_t = 1 - \frac{\sigma_t E_c^{-1}}{\varepsilon_t^{pl}\left(\frac{1}{b_t} - 1\right) + \sigma_t E_c^{-1}} \tag{10}$$

$$\varepsilon_t^{pl} = b_t\ \varepsilon_t^{in}$$

$$D_c = 1 - \frac{\sigma_c E_c^{-1}}{\varepsilon_c^{pl}\left(\frac{1}{b_c} - 1\right) + \sigma_c E_c^{-1}} \tag{11}$$

$$\varepsilon_c^{pl} = b_c\ \varepsilon_c^{in}$$

Where: D_t and D_c indicate the concrete tension and compression damage parameters, respectively; σ_c and σ_t denote the stress in compression and tension, respectively; ε_t^{pl} denotes the plastic strain associated with the tensile stress; ε_c^{pl} denotes the plastic strain associated with the compression stress; $b_c$and b_t are both constant values with a range ($0 < b_c,\ b_t < 1$).

5.3. Finite element type, interaction, and boundary condition

The NSC, UHPFRC jacket, and mechanical anchorage system ingredients are modelled using three-dimensional homogeneous stress 8-node linear brick elements (C3D8R) with reduced integration. The CFRP rods and reinforcing steel are formed as a 2-node linear 3-D truss solid element (T3D2) [42] to effectively represent their behavior, as shown in Fig. 18 (c). A sensitivity analysis mesh size of 20 mm was defined for the NSC, UHPFRC jacket, and mechanical system, as demonstrated in Fig. 18 (b). The "embedded region" constraint technique was employed to simulate a perfect bonding interaction contact between the rebar steel and CFRP rods with NSC and UHPFRC jacket, respectively. In addition, the model considered the interaction contact models between the NSC and UHPFRC jacket, as well as between the mechanical expansion anchor bolt and the NSC, UHPFRC jacket, and steel plate. These interaction models were modelled as surface-to-surface contact, with hard contact behavior in the normal direction and a specified coefficient of friction for the tangential direction [52]. Meanwhile, the interaction between the steel plate and the

bottom surface of the UHPFRC layer was defined as a "tie constraint" contact. The friction coefficient was considered 0.6 [52] between NSC and UHPFRC layers, and 0.7 at the interface between the mechanical anchorage system and NSC-UHPFRC layers [49]. Regarding the boundary condition, the support steel plates were coupled to the bottom surface using one reference point (RP1), while the loading steel plate was coupled to the top face (RP2). The support steel plates were restricted in translations and rotations in all three directions at the reference point. An incremental repeated (half-cyclic) analysis was performed using the explicit dynamic solver to verify the experimental test. The half-cycle displacements were determined by the amplitude of the cyclic frequency, as shown in Fig. 7.

5.4. Numerical results and verification

5.4.1. Load–displacement response

Table 10 provides a comprehensive summary of the FE results and validation with experimental work. Fig. 21 depicts the load versus deflection for the experimental work and FE simulations. From the results shown in Fig. 21, good agreement was observed between the experimental and FEM results. The FEM-SB1 model exhibited ductile behavior closely mirroring the experimental work, achieving an ultimate load of 168 kN, which closely approximated the experimental maximum load, as shown in Fig. 21 (a). However, the FEM-SB2 model's load-displacement curve showed reasonable agreement with the experimental result until the point of yielding steel reinforcement, which occurred at a load of roughly 200 kN, as illustrated in Fig. 21 (b). After the yield stage, the FEM-SB2 curve showed a slight drop until the failure phase compared to the EXP-SB2 slab. On the other hand, the FEM-SB2 model had a load-bearing capacity of 258 kN with a corresponding deflection of 26 mm, as shown in Table 10. In contrast, according to Fig. 21 (c), the load-displacement curve of the FEM-SB3 model showed a slight height compared to the experimental slab, beginning at a load of 130 kN until the failure stage. The FEM-SB3 model demonstrated an ultimate strength of 310 kN at a deflection of 22 mm, as illustrated in Table 10. Consequently, the overall ultimate load capacity of the FE models (FEM-SB2 and FEM-SB3) exceeded that of the experimental slabs (EXP-SB2 and EXP-SB3) by approximately 3 %. These differences in the results may be attributed to the disparities between the modeled boundary conditions in the software and the essential boundary conditions in the real world. Additionally, the coefficient of variation (COV) for FEM models in terms of peak load and midspan deflections was 0.033 and 0.052, respectively, as displayed in Table 10.

5.4.2. Failure mechanism and crack pattern

Fig. 22 presents the typical failure mechanisms observed in the FE models and the experimental work. The numerical models showed a high level of agreement with the experimental work regarding crack propagation and flexural damage patterns, as depicted in Fig. 22 (a, b, and c). For the control model SB1, failure initiated with the appearance of initial cracks on the bottom face of the slab, accompanied by spalling

Table 10
Summary of FE results and validation with experimental.

Slab	EXP		FEM			
ID	*Pu-e (KN)*	*Δu-e (mm)*	*Pu-f (KN)*	*Δu-f (mm)*	*Pu-e/ Pu-f*	*Δu-e/ Δu-f*
SB1	164	18	168	19.5	0.98	0.92
SB2	264	27	258	26	1.02	1.03
SB3	298	22.4	310	22	0.93	1.01
Average					0.97	0.98
SD					0.032	0.051
COV					0.033	0.052

Where: Pu-e represent the experimental maximum load; Δu-e represent the experimental deflection at maximum load; Pu-f represent the FE maximum load; Δu-f represent the FE deflection at maximum load.

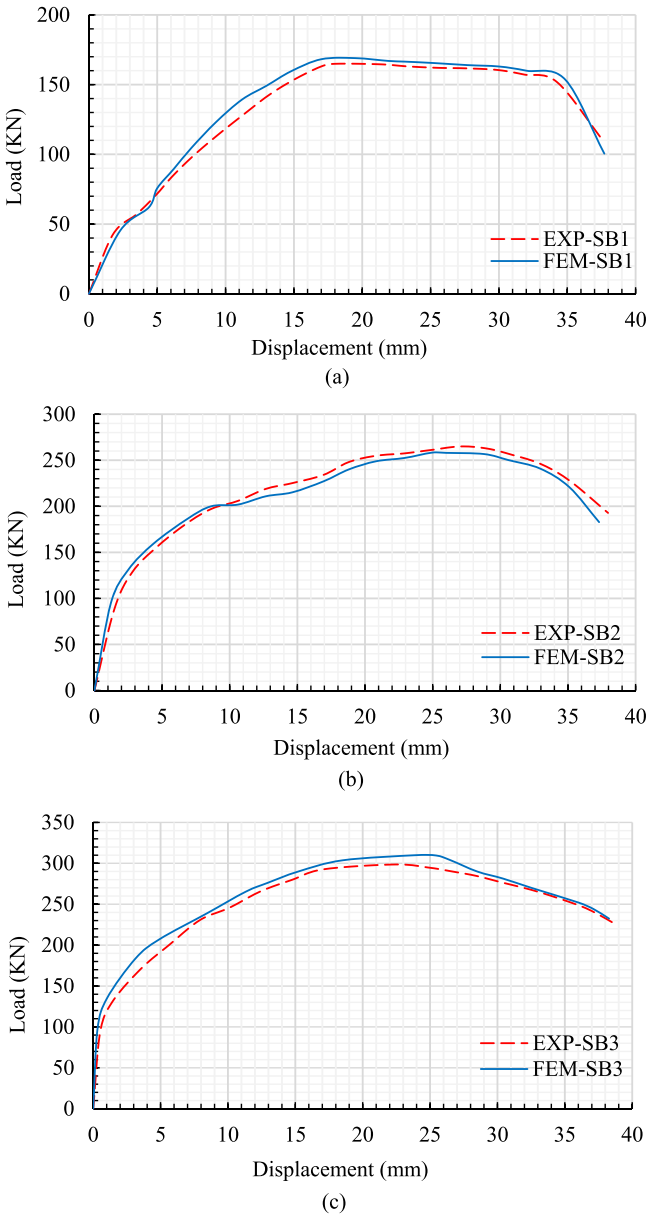

Fig. 21. Experimental and finite element load-deflection behavior.

of the cover, as shown in Fig. 22 (a). The bottom surface of the SB3 model exhibited regular cracks in two directions in the middle beside the mechanical systems, as represented in Fig. 22 (c). Furthermore, the plastic strain in the bottom middle surface of the SB3 model, particularly in the UHPFRC jacket, was more pronounced compared to that at the corners, as illustrated in Fig. 1(c). This indicates a higher tensile strain occurred in the central region of the model. Importantly, in the FEM-SB2 and FEM-SB3 models, no premature debonding occurred between the NSC and the UHPFRC jacket. Additionally, all mechanical anchorage systems remained securely in place without any slippage out of the slabs, as depicted in Fig. 22 (b and c). On the other hand, the reinforcing steel and CFRP mesh exhibited local buckling in the middle, illustrating the effective interface bonding technique with the NSC and UHPFRC layers, respectively, as depicted in Fig. 22 (e and d). In addition, the mechanical anchorage system exhibited a higher tensile plastic strain in the attached region of the NSC layer than in the UHPFRC region, as shown in Fig. 22 (g). This demonstrates the remarkable effectiveness of the mechanical anchorage system and the interaction approach in the strengthening strategy.

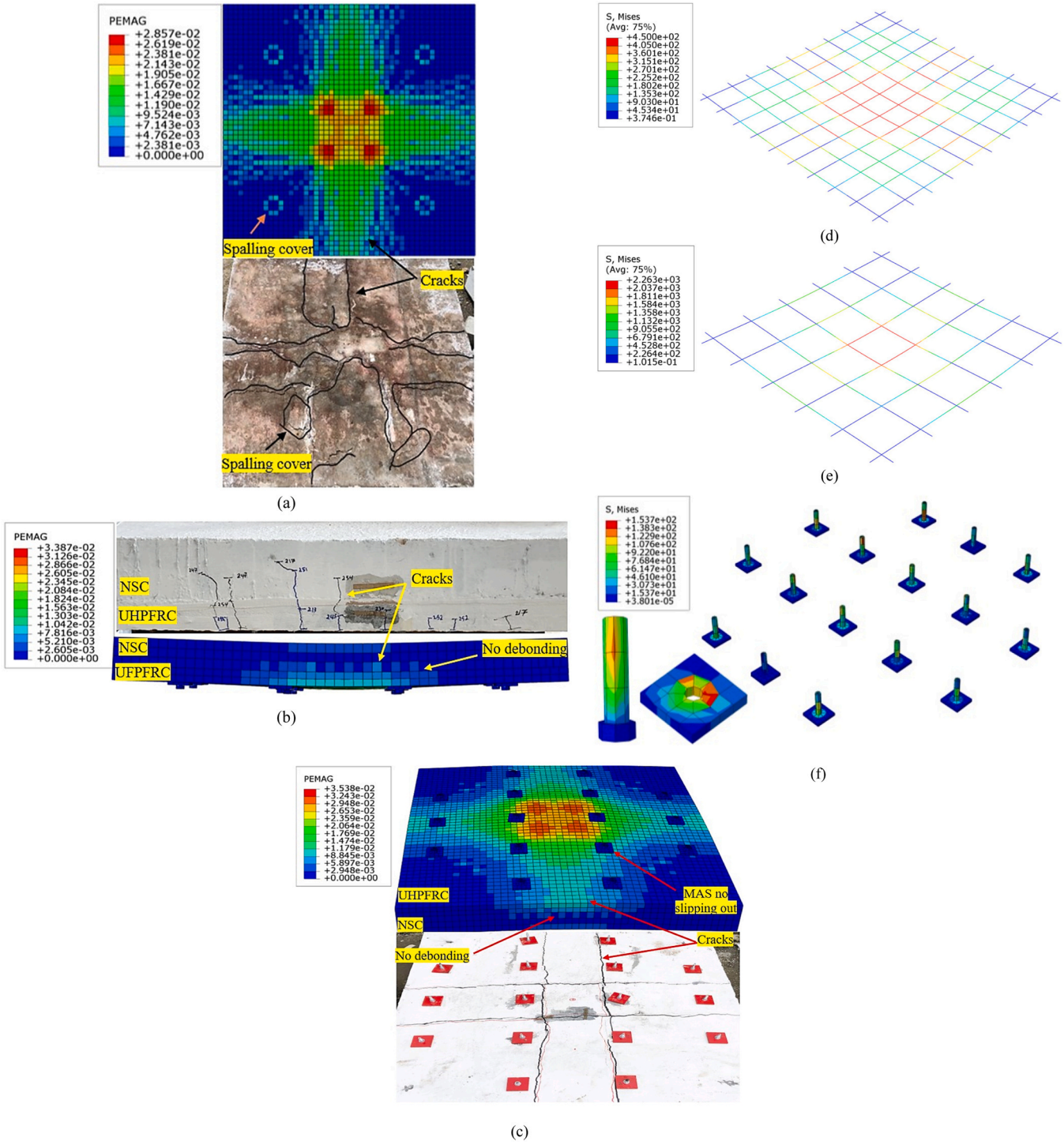

Fig. 22. Typical failure response: (a, b and c) validation between experimental and FE simulation for SB1, SB2 and SB3 slab, respectively; (d) reinforcing steel; (e) CFRP rods; (f) mechanical anchorage system.

5.4.3. Strain response

The ultimate strain in the reinforcing steel and CFRP rods obtained from the experimental work and FE simulation are listed in Table 11. Strain values in both rebar and CFRP rods were determined by calculating the average values of strain for the four bars in the middle. Fig. 23 represents the experimental and numerical load-strain relationship of the reinforcing steel and CFRP rod. From the FE results, the highest strain value in the reinforcing steel was recorded in the FEM-SB1 model, indicating that the rebar steel experienced more deformation under cyclic load. Conversely, the steel rebar in the FEM-SB3 model recorded an ultimate strain of 0.002637 mm, corresponding to an ultimate load of 310 kN, revealing a further reduction compared to both the FEM-SB1 and FEM-SB2 models, as shown in Table 11. This decrease is attributed to the presence of CFRP rods in the UHPFRC jacket, which allowed the reinforcing steel to better resist tensile stress. Generally, the variations between the results obtained through the finite element (FE) simulation and the experimental work were less than 7 %, as indicated in Table 11. This demonstrates that the FE models are highly accurate in predicting strain behavior.

Table 11
Ultimate strain of experimental and FE simulation.

Slab	Experimental		FE models		Difference	
	S-IC%	CFRP-IU %	S-ICF %	CFRP-IUF %	Steel rebar %	CFRP rod %
SB1	0.3474	-	0.3782		8.87	
SB2	0.3006	-	0.3192		6.18	
SB3	0.2485	0.3755	0.2637	0.3951	5.76	4.97

Where: S-IC and S-ICF represents the maximum strain of steel inside the concrete in the center for experimental and numerical, respectively; CFRP-IU and CFRP-IUF represents the maximum strain of CFRP rod inside the UHPFRC jacket at the center for experimental and numerical, respectively.

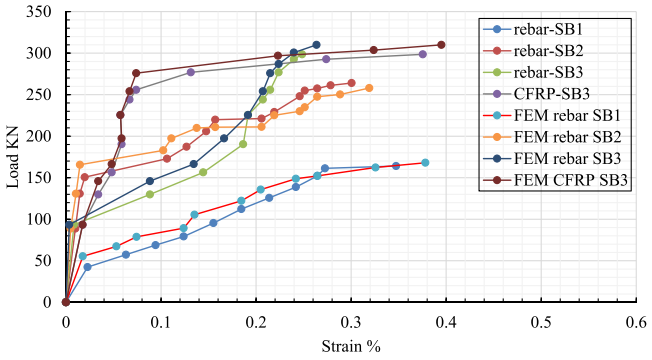

Fig. 23. Experimental and numerical Load-strain relationship for rebar steel and CFRP rods.

Table 12
FE simulation results.

Slab ID	Pu (kN)	Δy (mm)	Δu (mm)	Ductility (Δu/Δy)	Stiffness (kN/mm)
FEM-SB1	168	17.4	19.5	1.12	8.6
FEM-SB2	258	13.4	26	1.95	9.92
FEM-SB3	310	10.6	22	2.07	14

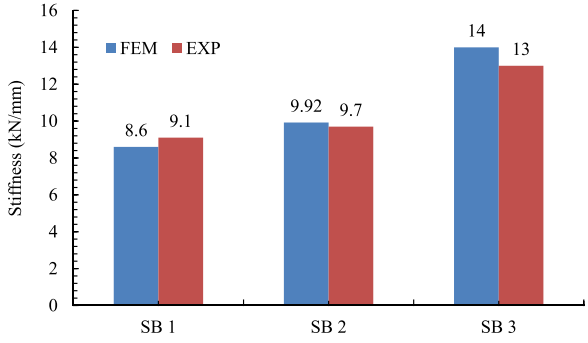

Fig. 24. Elastic stiffness for the experimental work and numerical.

5.4.4. Ductility and elastic stiffness of FE model

Table 12 shows the ductility (μ) and elastic stiffness (K) values for each finite element (FE) model. Fig. 24 provides a comparison of stiffness between the FE simulation and experimental data. Ductility describes the plastic deformation of a slab starting from the yielding phase, as calculated from Eq. 1. Moreover, the ductility index values of the FE models were slightly higher than those of the experimental specimens. At maximum load, the overall ductility performance of the FE models was 4 %. On the other hand, the elastic stiffness is determined by the slope of the linear part of the load-deflection curve. Specifically, the stiffness strengths of the FEM-SB2 and FEM-SB3 models were 9.92 kN/mm and 14 kN/mm, respectively, while the FEM-SB1 model exhibited a stiffness strength of 8.6 kN/mm, as detailed in Table 12. Consequently, the overall stiffness of the FE models exhibited a 2.7 % increase compared to the experimental results. These FE values for ductility and elastic stiffness demonstrate that closely align with the experimental outcomes.

6. Parametric study

Parametric studies were conducted on strengthened RC slabs using CFRP rods and UHPFRC jackets with mechanical anchorage system to investigate their effect on the resistance of the strengthened slab under repetitive incremental cyclic loads. The considered parameters included the impact number of the mechanical anchorage system, the effect of UHPFRC thickness, and the effect of CFRP rod diameter, as shown in Table 13.

6.1. Effect of number of mechanical anchorage system

Two FE models were developed to assess the effect of the number of mechanical anchorage systems on the strengthened slabs, as shown in Fig. 25. The first model (M25) included twenty-five units of the mechanical anchorage system, while the second model (M30) had thirty units, as detailed in Table 13. As depicted in Table 14, the finite element (FE) analysis results demonstrated that the number of mechanical anchorage systems significantly enhanced the proposed strengthened system. Fig. 26 illustrates the Load-displacement curve of FE models with various numbers of mechanical anchorage systems. Increasing the number of mechanical anchorage systems in the M25 and M30 models improved the maximum load by 13.2 % and 18.4 %, respectively, as shown in Fig. 26. Furthermore, the slabs exhibited an 11 % increase in stiffness compared to the experimental specimens. Overall, the increased number of mechanical systems enabled the CFRP rods and UHPFRC jacket to better resist loads, thereby reducing the risk of early debonding.

6.2. Effect of UHPFRC jacket thickness

Fig. 27 displays the load-deflection relationship of two different finite element models designed to evaluate the impact of UHPFRC jacket thickness on the strengthened slab. The UHPFRC jacket thicknesses of 30 mm and 40 mm were examined, as shown in Table 13. The results from Fig. 27 indicate that a decrease in UHPFRC jacket thickness affected on the flexural strength of the strengthened models. The FE models with jacket thicknesses of 30 mm and 40 mm experienced a 6.5 % and 4 % reduction in peak load, respectively. On the other hand, the deflections increased by 5 % and 3 %, respectively. This highlights that reducing the thickness of the UHPFRC jacket leads to a decrease in the stiffness of the specimens.

Table 13
Parameters of the parametric investigations.

Group	Slab ID	UHPFRC thickness (mm)	Variable
Group1	SB2-M25	50	Number mechanical system
	SB2-M30	50	Number mechanical system
	SB3-M25	50	Number mechanical system
	SB3-M30	50	Number mechanical system
Group2	SB2–30	30	UHPFRC thickness
	SB2–40	40	UHPFRC thickness
	SB3–30	30	UHPFRC thickness
	SB3–40	40	UHPFRC thickness
Group3	SB3-D10	50	CFRP diameters
	SB3-D12	50	CFRP diameters

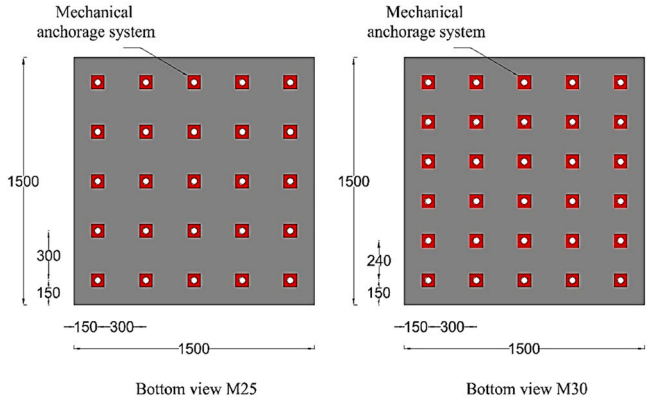

Fig. 25. Distribution details of the mechanical system.

Table 14
Results of the parametric study.

Group	Slab ID	*PL (KN)*	*Δm (mm)*	*Stiffness (KN/mm)*
Group1	SB2-M25	293	26.6	11.01
	SB2-M30	302	26.23	11.5
	SB3-M25	345.2	24.3	14.2
	SB3-M30	355	24.6	14.4
Group2	SB2–30	247.4	30.1	8.21
	SB2–40	253.21	29.4	8.61
	SB3–30	278.14	28.7	9.7
	SB3–40	286.5	28	10.23
Group3	SB3-D10	318.4	21.6	14.7
	SB3-D12	325	20.2	16.1

PL: denotes the numerical peak load; *Δm* denotes the numerical mid-span deflection corresponding to peak load.

6.3. Effect of CFRP rods diameter

The impact of the CFRP bar diameter on the proposed strengthening system was assessed using CFRP rod diameters of 10 mm and 12 mm, as represented in Table 13. Fig. 28 displays the load-displacement curves for the FE models with different CFRP rod diameters. In the model with CFRP rod diameters of 10 mm, the maximum load increased from 298 kN to 318.4 kN, corresponding to a deflection of 21.6 mm. In contrast, the ultimate load of SB3-D12 model increased to 325 kN with a deflection of 20.2 mm, as shown in Table 14. Increasing the cross-sectional areas of the CFRP rods (D10 and D12) resulted in an increase in the peak load by 6.85 % and 9.06 %, respectively, compared to the experimental work (D8). Overall, these results indicate that increasing the cross-sectional area of the CFRP rods has a noticeable effect on the proposed strengthening system.

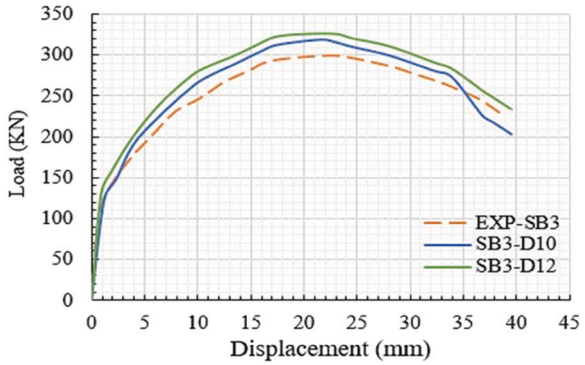

Fig. 28. Load-displacement curve of FE models with different CFRP rod diameters.

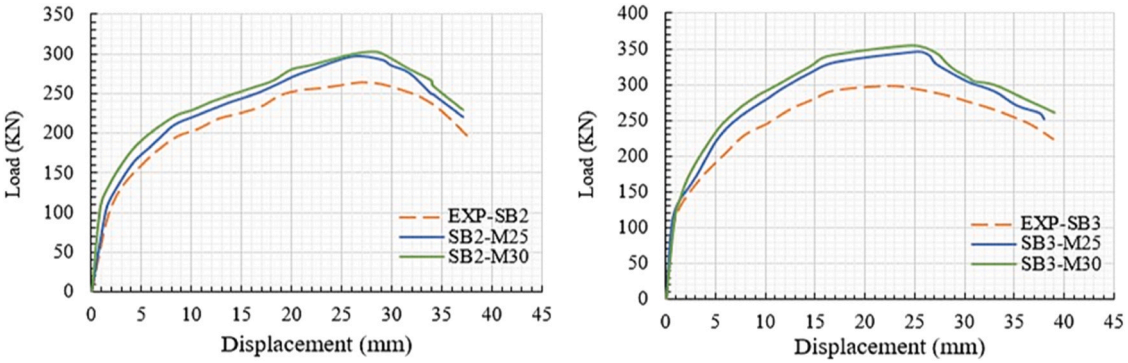

Fig. 26. Load-displacement curve of FE models with different numbers of mechanical anchorage systems.

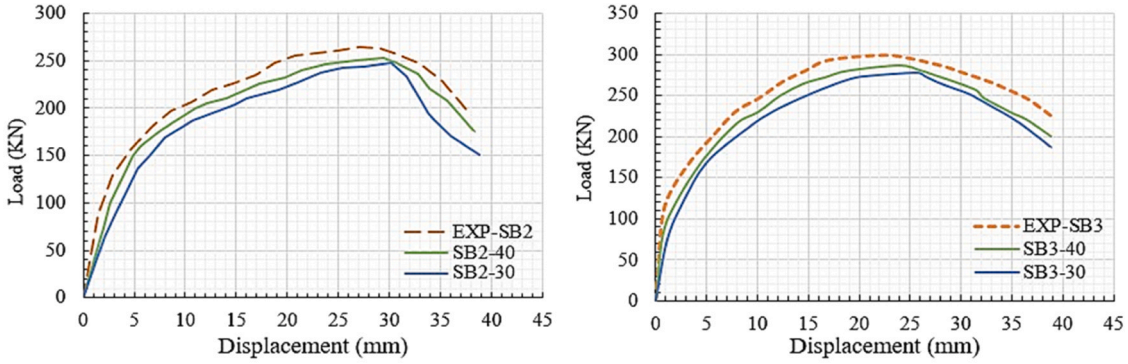

Fig. 27. Load-displacement curve of FE models with different UHPFRC jacket thickness.

7. Design model of strengthened slab

An analytical/mechanistic model was used to analyze the moment capacity of the strengthened RC slab using CFRP bars and a UHPFRC jacket with a mechanical anchorage system. This study employed internal stresses based on the simple plastic theory of a composite model to accurately predict internal forces. The collapse moment was determined by analyzing the internal forces in the slab at the specific cross-section in a state of equilibrium. Fig. 29 illustrates the analytical design model of the strengthened slab. In the design model scheme, the CFRP rods and the reinforcing steel were assumed in the tension phase, as shown in Fig. 29. The Whitney stress block, an equivalent rectangular stress distribution, was used to represent concrete in compression, following the guidelines of ACI Code Section 10.2.7. Furthermore, in the design model, the tension stress distributed equally along the UHPFRC jacket, as shown in Fig. 29. The value of (X_0), which illustrates the NSC depth in the compression zone, is determined from axial force equilibrium, as simplified in Eq. 12. Additionally, the mechanical anchorage bolts' contribution to this design model is determined by their shear resistance. The shear resistance of a mechanical anchorage bolt is calculated using Eq. 13. The flexural moment capacity of the strengthened slab was obtained by evaluating the moment of force around the point of the neutral axis. Hence, the flexural moment capacity (Mu) can be expressed as in Eq. 14.

$$X_0 = \frac{Au\,fut + fy\,Auct + fy\,As}{fcb} \tag{12}$$

$$V = Ab\,fv \tag{13}$$

$$Mu = \frac{fcb\quad x_0^2}{2} + f_{ut}\quad b\quad h_1\left(h_3 - \frac{h_1}{2}\right) + fy\,Acu(h3 - a_1) + fy\,As(h3 - h1 - a_2) + V \tag{14}$$

where (Tu) represents tensile forces in the UHPFRC jacket; (Tuc) denotes the tensile forces in CFRP rods; (Tus) demonstrates the tensile forces of reinforcing steel (Cuc) represents the compressive forces in the reinforced concrete slab; (Ab) denotes the cross-sectional area of the bolt and (fv) denotes the shear strength of the expansion bolt; *As*and*Acu* denotes the cross-section area rebar steel and CFRP rods, respectively.

7.1. Validation of design model

Eq. (14) was used to calculate the flexural moment capacity of strengthened slab. The design model approach results were compared with both experimental and FE simulation results in Table 15. Additionally, Table 15 includes a comparison of the design model results with experimental data from the literature (Hor Yin [34]) to validate the applicability of this formula for calculating the flexure moment capacity of strengthened slabs. The results of the design model showed good agreement with the relevant experimental work and FE simulations, with the coefficient of variation (COV) ranging from 2.92 % to 6.05 %, as indicated in Table 15. The results demonstrate that Eqs. (12) and (14) can be potentially employed to predict the ultimate flexure capacity of reinforced concrete slabs strengthened using CFRP rods and UHPFRC jackets with a mechanical anchorage system.

Table 15
Validation between the experimental, FE simulation and the design models.

Item	M Exp. KN.m	M Cal. KN.m	M FE. KN.m	Exp/ Cal	FE/ Cal.	Hor Yin [34]	COV %
SB1	53.3	47.4	54.6	1.124	1.152	RE-0 (0.995)	6.28
SB2	85.8	81.3	83.8	1.055	1.03	OV-50 (1.106)	2.96
SB3	96.85	100.7	101	0.961	1.003	OV-50a (1.032)	2.92

8. Cost analysis and compatibility with other reinforcement techniques

A detailed cost-benefit analysis of the proposed strengthening technique applying a UHPFRC jacket with CFRP bars and bonded by mechanical anchorage bolts requires a comprehensive consideration of various factors over the lifespan of the reinforcement such as cost and maintenance. This section provides a detailed study of the cost of the proposed new system as well as its lifespan and maintenance. Table 16 provides the most precise information on the total cost of the proposed system. Initial costs encompass material procurement, equipment, and specific attention to the installation of the UHPFRC jacket, CFRP bars, and anchorage bolts. According to Table 16, the cost of executing the proposed system, which has dimensions of (1500×1500×50) mm, is 921.9 $. This cost does not include any additional implementation charges because the work was carried out within the university's laboratories. When comparing the proposed strengthening system with other modern systems, for example, pre-tensioning, notice that the cost is less, and the advantage of the proposed system is the longer life of the structure and the possibility of easy maintenance by replacing the

Table 16
Details cost of the strengthening proposed system.

Items	UHPFRC (kg/m3)	CFRP rods (kg)	MEABS kg	Plate kg	
Weight	285	5	3.5	12	
Cost ($)	2400	24.5	17.2	4.6	
Total cost ($)	684	122.5	60.2	55.2	921.9 $

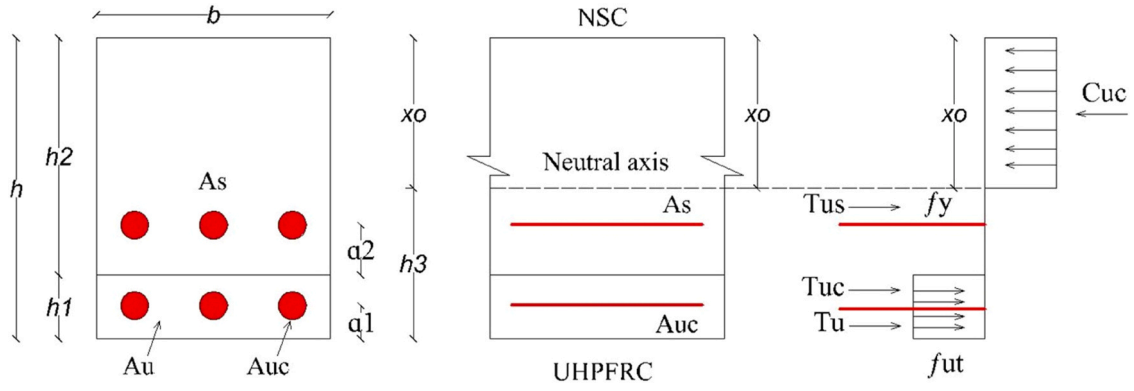

Fig. 29. Scheme design model of the strengthened slab.

mechanical system. The estimated lifespan of the proposed reinforcement system is 50 years, resulting in an annual maintenance cost of 18.5 $. Additionally, possible savings in repair costs are factored into the analysis, accounting for the reinforcement's ability to mitigate damage and extend the slab's service life. This comprehensive approach to cost-benefit analysis provides decision-makers with useful information about the long-term financial implications of implementing the recommended strengthening technique. On the other hand, iintegrating the proposed strengthening method with external post-tensioning devices is a viable way to improve the structural performance of RC slabs. External post-tensioning is the process of putting high-strength tendons (CFRP) or cables (steel) on the surface of a slab and applying tensile stresses to improve load-carrying capacity and regulate deflections. By combining external post-tensioning with the UHPFRC jacket, synergistic effects can be achieved, improving the overall structural behavior of the slab. The UHPFRC jacket, when combined with the mechanical system, enhances the slab's resistance to cracking and improves the performance of the post-tensioning system by providing additional confinement.

9. Conclusion

This study presented a new scheme for strengthening RC slabs through the utilization of UHPFRC jackets and CFRP rods anchored using mechanical expansion anchor bolts and carbon steel plates. Accordingly, the experimental tests have been conducted on the strengthened beams using the proposed method by applying half-cyclic loads using a dynamic actuator, and the results have been investigated. The subsequent conclusions were drawn based on the experimental results:

- The UHPFRC jackets significantly contributed to enhanced cracking loads and delayed the development of cracks on the bottom surface of strengthened slabs. The initial cracking load in the strengthened slabs (SB2 and SB3) exhibited an average increase of 82 %.
- The study revealed that combining the CFRP rod and the UHPFRC jacket with a mechanical anchorage system significantly decreased the width and number of cracks in the strengthened slabs (SB2 and SB3).
- Furthermore, the capacity of the slabs increased in both SB2 and SB3 slabs.
- Slabs SB2 and SB3 experienced an increase in ultimate load of 61 % and 82 %, respectively.
- Embedding of carbon fiber reinforced polymer (CFRP) bars within the UHPFRC jacket in the SB3 slab led to a notable enhancement of 13 % in the ultimate load capacity as compared to the SB2 slab.
- The steel plates used as a part of the mechanical anchorage system played a crucial role in distributing the load applied by the mechanical expansion anchorage bolt across a broader surface area of the slabs, preventing localized stress concentrations that might otherwise contribute to slab deformation and slip the bolts.
- Importantly, none of the mechanical anchorage systems exhibited any slipping out of the slabs during the test, signifying the effectiveness and reliability of the proposed strengthening system.
- Notably, the proposed strengthening method succeeded and effectively eliminated the issue of premature debonding. In the SB3 and SB2 slabs, no debonding was shown between the reinforced concrete slabs and the UHPFRC jackets until the point of failure.
- The strengthened slabs (SB2 and SB3) demonstrated good results in terms of ductility behavior compared to the control slab SB1.
- The energy absorption capacity of the strengthened slabs (SB2 and SB3) increased by an average of 85 % and 95 %, respectively, compared to the SB1 slab.
- The maximum strain of reinforcement steel decreased by an average of 14 % and 18 % in the SB2 and SB3 slabs, respectively, compared to the SB1 slab.
- The finite element modeling (FEM) results showed a high level of agreement with the experimental results. The FE models accurately predicted the maximum load and deflection behavior, closely matching the values obtained from experimental tests.
- Increasing the number of mechanical anchorage systems enhanced both the ductility and stiffness of the slabs.
- Decreasing the UHPFRC jacket thickness slightly reduced the overall ultimate load and deflection response.
- Increasing the cross-sectional areas of the CFRP rods led to an 8 % increase in peak load capacity.
- The developed design model presents good estimates of the moment capacity of the strengthened slabs.
- Accordingly, it is recommended to further investigate the application of the newly proposed strengthening method on other reinforced concrete members like beams and columns, which this technique has the potential to greatly enhance the capacity of the reinforced concrete members and prevent early de-bonding.

CRediT authorship contribution statement

Firas Hassan Saeed: Writing – original draft, Visualization, Software, Methodology, Investigation, Formal analysis, Conceptualization. **Farzad Hejazi:** Writing – review & editing, Visualization, Validation, Supervision, Software, Resources, Project administration, Methodology, Investigation, Funding acquisition, Formal analysis, Data curation, Conceptualization. **Raizal Saifulnaz Muhammad Rashid:** Validation, Resources, Conceptualization.

Declaration of Competing Interest

The authors declare that they have no known competing financial interests or personal relationships that could have appeared to influence the work reported in this paper.

Data availability

No data was used for the research described in the article.

References

[1] S.E. El-Gamal, A. Al-Nuaimi, A. Al-Saidy, A. Al-Lawati, Efficiency of near surface mounted technique using fiber reinforced polymers for the flexural strengthening of RC beams, Constr. Build. Mater. vol. 118 (2016) 52–62, https://doi.org/10.1016/j.conbuildmat.2016.04.152.
[2] T.G. Wakjira, U. Ebead, Hybrid NSE/EB technique for shear strengthening of reinforced concrete beams using FRCM: experimental study, Constr. Build. Mater. vol. 164 (2018) 164–177, https://doi.org/10.1016/j.conbuildmat.2017.12.224.
[3] R.A. Hawileh, W. Nawaz, J.A. Abdalla, Flexural behavior of reinforced concrete beams externally strengthened with Hardwire Steel-Fiber sheets, Constr. Build. Mater. vol. 172 (2018) 562–573, https://doi.org/10.1016/j.conbuildmat.2018.03.225.
[4] S. Seręga, D.H. Faustmann, Flexural strengthening of reinforced concrete beams using external tendons, Eng. Struct. vol. 252 (November 2021) (2022), https://doi.org/10.1016/j.engstruct.2021.113277.
[5] Z. Zhu, E. Zhu, Y. Ni, D. Li, Flexural fatigue behavior of large-scale beams strengthened with side near surface mounted (SNSM) CFRP strips, Eng. Struct. vol. 180 (June 2018) (2019) 134–147, https://doi.org/10.1016/j.engstruct.2018.11.039.
[6] W.T. Jung, J.S. Park, J.Y. Kang, M.S. Keum, Y.H. Park, Flexural behaviour of RC beams strengthened with prestressed CFRP NSM tendon using new prestressing system, Int. J. Polym. Sci. vol. 2017 (2017), https://doi.org/10.1155/2017/1497349.
[7] N. Attari, S. Amziane, M. Chemrouk, Flexural strengthening of concrete beams using CFRP, GFRP and hybrid FRP sheets, Constr. Build. Mater. vol. 37 (2012) 746–757, https://doi.org/10.1016/j.conbuildmat.2012.07.052.
[8] M. Aslam, P. Shafigh, M.Z. Jumaat, S.N.R. Shah, Strengthening of RC beams using prestressed fiber reinforced polymers - a review, Constr. Build. Mater. vol. 82 (2015) 235–256, https://doi.org/10.1016/j.conbuildmat.2015.02.051.
[9] H.M. Afefy, K. Sennah, H. Akhlagh-Nejat, Experimental and analytical investigations on the flexural behavior of CFRP-strengthened composite girders, J. Constr. Steel Res. vol. 120 (2016) 94–105, https://doi.org/10.1016/j.jcsr.2016.01.010.

[10] R. El-Hacha, K. Soudki, Prestressed near-surface mounted fibre reinforced polymer reinforcement for concrete structures - a review, Can. J. Civ. Eng. vol. 40 (11) (2013) 1127–1139, https://doi.org/10.1139/cjce-2013-0063.
[11] X.F. Nie, S.S. Zhang, J.G. Teng, Strengths of RC beams with a fibre-reinforced polymer (FRP)-strengthened web opening, Compos. Struct. vol. 258 (December 2020) (2021) 113380, https://doi.org/10.1016/j.compstruct.2020.113380.
[12] J.G. Teng, T. Yu, D. Fernando, Strengthening of steel structures with fiber-reinforced polymer composites, J. Constr. Steel Res. vol. 78 (2012) 131–143, https://doi.org/10.1016/j.jcsr.2012.06.011.
[13] M.M. Ism, M. Rabie, Flexural behavior of continuous RC beams strengthened with externally bonded CFRP sheets, Alex. Eng. J. vol. 58 (2) (2019) 789–800, https://doi.org/10.1016/j.aej.2019.07.001.
[14] I.F. Kara, A.F. Ashour, M.A. Köroğlu, Flexural performance of reinforced concrete beams strengthened with prestressed near-surface-mounted FRP reinforcements, Compos. Part B Eng. vol. 91 (2016) 371–383, https://doi.org/10.1016/j.compositesb.2016.01.023.
[15] I.A. Sharaky, L. Torres, J. Comas, C. Barris, Flexural response of reinforced concrete (RC) beams strengthened with near surface mounted (NSM) fibre reinforced polymer (FRP) bars, Compos. Struct. vol. 109 (1) (2014) 8–22, https://doi.org/10.1016/j.compstruct.2013.10.051.
[16] S. Reichenbach, P. Preinstorfer, M. Hammerl, B. Kromoser, A review on embedded fibre-reinforced polymer reinforcement in structural concrete in Europe, Constr. Build. Mater. vol. 307 (April) (2021) 124946, https://doi.org/10.1016/j.conbuildmat.2021.124946.
[17] D.S. Yang, S.K. Park, K.W. Neale, Flexural behaviour of reinforced concrete beams strengthened with prestressed carbon composites, Compos. Struct. vol. 88 (4) (2009) 497–508, https://doi.org/10.1016/j.compstruct.2008.05.016.
[18] A. Nabil, H.M. Afefy, N.M. Kassem, Ultimate capacity of reinforced concrete castellated beams subjected to external pre-stressing, Eng. Struct. vol. 250 (December 2020) (2022) 113471, https://doi.org/10.1016/j.engstruct.2021.113471.
[19] L. De Lorenzis, J.G. Teng, Near-surface mounted FRP reinforcement: an emerging technique for strengthening structures, Compos. Part B Eng. vol. 38 (2) (2007) 119–143, https://doi.org/10.1016/j.compositesb.2006.08.003.
[20] H.B. Park, J.S. Park, J.Y. Kang, W.T. Jung, Fatigue behavior of concrete beam with prestressed near-surface mounted CFRP reinforcement according to the strength and developed length, Materials vol. 12 (1) (2018), https://doi.org/10.3390/ma12010051.
[21] G.M. Dalfré, J.A.O. Barros, NSM technique to increase the load carrying capacity of continuous RC slabs, Eng. Struct. vol. 56 (2013) 137–153, https://doi.org/10.1016/j.engstruct.2013.04.021.
[22] M.R.F. Coelho, J.M. Sena-Cruz, L.A.C. Neves, M. Pereira, P. Cortez, T. Miranda, Using data mining algorithms to predict the bond strength of NSM FRP systems in concrete, Constr. Build. Mater. vol. 126 (2016) 484–495, https://doi.org/10.1016/j.conbuildmat.2016.09.048.
[23] Y. Lv, P. Wu, J. Chou, W. Han, M. Su, H. Peng, An experimental study on the interfacial bonding performance of horizontally embedded CFRP strips to concrete, Constr. Build. Mater. vol. 369 (February) (2023) 130514, https://doi.org/10.1016/j.conbuildmat.2023.130514.
[24] T.J. Mohammed, B.H. Abu Bakar, N. Muhamad Bunnori, Torsional improvement of reinforced concrete beams using ultra high-performance fiber reinforced concrete (UHPFC) jackets - Experimental study, Constr. Build. Mater. vol. 106 (2016) 533–542, https://doi.org/10.1016/j.conbuildmat.2015.12.160.
[25] C. Oesterlee, "Structural analysis of a composite bridge girder combining UHPFRC and reinforced concrete," … *High Perform. Concr.* …, pp. 1–8, 2008, [Online]. Available: http://infoscience.epfl.ch/record/133586/files/Paper FE analysis UHPFRC CO HS EB.pdf.
[26] T. Noshiravani, E. Brühwiler, Rotation capacity and stress redistribution ability of R-UHPFRC-RC composite continuous beams: an experimental investigation, Mater. Struct. Constr. vol. 46 (12) (2013) 2013–2028, https://doi.org/10.1617/s11527-013-0033-5.
[27] D.Y. Yoo, N. Banthia, Mechanical and structural behaviors of ultra-high-performance fiber-reinforced concrete subjected to impact and blast, Constr. Build. Mater. vol. 149 (2017) 416–431, https://doi.org/10.1016/j.conbuildmat.2017.05.136.
[28] J. Li, C. Wu, H. Hao, Investigation of ultra-high performance concrete slab and normal strength concrete slab under contact explosion, Eng. Struct. vol. 102 (2015) 395–408, https://doi.org/10.1016/j.engstruct.2015.08.032.
[29] S.A. Paschalis, A.P. Lampropoulos, O. Tsioulou, Experimental and numerical study of the performance of ultra high performance fiber reinforced concrete for the flexural strengthening of full scale reinforced concrete members, Constr. Build. Mater. vol. 186 (2018) 351–366, https://doi.org/10.1016/j.conbuildmat.2018.07.123.
[30] M. Safdar, T. Matsumoto, K. Kakuma, Flexural behavior of reinforced concrete beams repaired with ultra-high performance fiber reinforced concrete (UHPFRC), Compos. Struct. vol. 157 (2016) 448–460, https://doi.org/10.1016/j.compstruct.2016.09.010.
[31] D.Y. Yoo, N. Banthia, S.W. Kim, Y.S. Yoon, Response of ultra-high-performance fiber-reinforced concrete beams with continuous steel reinforcement subjected to low-velocity impact loading, Compos. Struct. vol. 126 (2015) (2015) 233–245, https://doi.org/10.1016/j.compstruct.2015.02.058.
[32] T. Noshiravani, E. Brühwiler, Experimental investigation on reinforced ultra-high-performance fiber-reinforced concrete composite beams subjected to combined bending and shear, Acids Struct. J. vol. 110 (2) (2013) 251–261, https://doi.org/10.14359/51684405.
[33] A.P. Lampropoulos, S.A. Paschalis, O.T. Tsioulou, S.E. Dritsos, Strengthening of reinforced concrete beams using ultra high performance fibre reinforced concrete (UHPFRC), Eng. Struct. vol. 106 (2016) 370–384, https://doi.org/10.1016/j.engstruct.2015.10.042.
[34] H. Yin, W. Teo, K. Shirai, Experimental investigation on the behaviour of reinforced concrete slabs strengthened with ultra-high performance concrete, Constr. Build. Mater. vol. 155 (2017) 463–474, https://doi.org/10.1016/j.conbuildmat.2017.08.077.
[35] B. Pan, F. Liu, Y. Zhuge, J.J. Zeng, J.J. Liao, ECCs/UHPFRCCs with and without FRP reinforcement for structural strengthening/repairing: a state-of-the-art review, Constr. Build. Mater. vol. 316 (December 2021) (2022) 125824, https://doi.org/10.1016/j.conbuildmat.2021.125824.
[36] Z. Pedram, Y. Xiong, J. Xin, M. Amir, Punching shear enhancement of flat slabs with partial use of ultrahigh-performance concrete,, J. Mater. Civ. Eng. vol. 27 (9) (Sep. 2015) 4014255, https://doi.org/10.1061/(ASCE)MT.1943-5533.0001219.
[37] ACI Committee 355, Guide for design of anchorage to concrete: Examples using ACI 318 appendix D. 2011.
[38] T. Datasheet, "Hilti Hst3 Expansion Anchor."
[39] S. Bars *et al.*, "Standard Specification for General Requirements for Steel Bars, Carbon and Alloy, Hot-Wrought 1 Title of Specification ASTM Designation A," vol. i, pp. 1–16, 2013, doi: 10.1520/A0029.
[40] P.D. Sheet, "Sika ® CarboDur ® BC 8," no. October, pp. 8–10, 2023.
[41] R.A. Hawileh, H.A. Rasheed, J.A. Abdalla, A.K. Al-Tamimi, Behavior of reinforced concrete beams strengthened with externally bonded hybrid fiber reinforced polymer systems, Mater. Des. vol. 53 (2014) 972–982, https://doi.org/10.1016/j.matdes.2013.07.087.
[42] C.A.E. User, Abaqus theory manual," *Abaqus 6.13 Doc.*, no, Dassault Systemes Simulia Corp, Providence, RI, USA, 2014.
[43] M.B. Zidani, K. Belakhdar, A. Tounsi, E.A. Adda Bedia, Finite element analysis of initially damaged beams repaired with FRP plates, Compos. Struct. vol. 134 (March) (2015) 429–439, https://doi.org/10.1016/j.compstruct.2015.07.124.
[44] Y.T. Obaidat, S. Heyden, O. Dahlblom, The effect of CFRP and CFRP/concrete interface models when modelling retrofitted RC beams with FEM, Compos. Struct. vol. 92 (6) (2010) 1391–1398, https://doi.org/10.1016/j.compstruct.2009.11.008.
[45] P. Ayough, N.H.R. Sulong, Z. Ibrahim, Analysis and review of concrete-filled double skin steel tubes under compression, Thin-Walled Struct. vol. 148 (December 2019) (2020) 106495, https://doi.org/10.1016/j.tws.2019.106495.
[46] GB, National standard of the People's Republic of China - code for design of concrete structures,", Construction vol. Beijing (2002) 64–73.
[47] L. Jia, Z. Fang, Z. Huang, K. Pilakoutas, Q. Wang, X. Tan, Flexural behavior of uhpc beams prestressed with external cfrp tendons, Appl. Sci. vol. 11 (19) (2021), https://doi.org/10.3390/app11199189.
[48] M. Asadi, E Xperimental test and F inite E lement M odelling of pedestrian, Test (Fig. 1) (2010) 60876.
[49] L.R. dos Santos, H. de S. Cardoso, R.B. Caldas, L.F. Grilo, Finite element model for bolted shear connectors in concrete-filled steel tubular columns, Eng. Struct. vol. 203 (April 2019) (2020) 109863, https://doi.org/10.1016/j.engstruct.2019.109863.
[50] M. de F.F. Chaves, E.M. Xavier, A.M.C. Sarmanho, J.G. Ribeiro Neto, Study of bolts used as shear connectors in concrete-filled steel tubes, Eng. Struct. vol. 231 (December 2020) (2021), https://doi.org/10.1016/j.engstruct.2020.111697.
[51] P. Ayough, Y.H. Wang, W. Zeng, Q.Q. Liang, M. Elchalakani, C. Zou, Numerical investigation and design of UHPC-encased CFST stub columns under axial compression, Eng. Struct. vol. 302 (November 2023) (2024) 117387, https://doi.org/10.1016/j.engstruct.2023.117387.
[52] S. Ahmed, E.Y. Mohamed, H.A. Mohamed, M. Emara, Experimental and numerical investigation of flexural behavior of RC beams retrofitted with reinforced UHPFRC layer in tension surface, Structures vol. 49 (January) (2023) 106–123, https://doi.org/10.1016/j.istruc.2023.01.113.